BRNO UNIVERSITY OF TECHNOLOGY

VYSOKÉ UČENÍ TECHNICKÉ V BRNĚ

CENTRAL EUROPEAN INSTITUTE OF TECHNOLOGY BUT

STŘEDOEVROPSKÝ TECHNOLOGICKÝ INSTITUT VUT

DEVELOPMENT OF A NOVEL TERAHERTZ MAGNETIC RESONANCE SPECTROMETER FOR SPIN DYNAMICS INVESTIGATIONS

VÝVOJ NOVÉHO SPEKTROMETRU MAGNETICKÉ REZONANCE V TERAHERTZOVÉM ROZSAHU PRO VÝZKUM DYNAMIKY SPINŮ

DOCTORAL THESIS

DIZERTAČNÍ PRÁCE

AUTHOR

AUTOR PRÁCE

Ing. Antonín Sojka

SUPERVISOR

ŠKOLITEL

doc. Ing. Petr Neugebauer, Ph.D.

CO-SUPERVISOR

ŠKOLITEL SPECIALISTA

Dr. Oleksii Laguta

CO-SUPERVISOR

ŠKOLITEL SPECIALISTA

Dr. Vinicius Tadeu Santana

BRNO 2022

ABSTRACT

During the last decades, the method called High Frequency/Field Electron Paramagnetic Resonance (HF-EPR) spectroscopy experienced a boom in chemistry, biology, material science, and physics. Still, HF-EPR spectrometers operating at sub-THz frequencies are mostly custom-made with non-standard solutions. The thesis aims to develop a novel broadband EPR spectrometer capable of operating in the field and frequency domain and performing frequency domain rapid scan to study relaxation times. The spectrometer operates at high magnetic fields up to 16 T, broad frequency range from 90 to 1100 GHz, and temperature ranges of 4 — 400 K. Furthermore, The work describes the design and development of six different exchangeable sample holders with a proof-of functionality measurement and unique fast-loading flange for the sample holder. The capability of the spectrometer to perform Rapid Scan measurement is demonstrated in the measurements of the LiPc single crystal and the DPPH sample dissolved in toluene.

KEYWORDS

Electron Paramagnetic Resonance, Electron Spin Resonance, EPR, ESR, High frequencies/fields, HF-EPR, Rapid scan, EPR sample holder

ABSTRAKT

Během posledních desetiletí zaznamenala metoda nazývaná vysokofrekvenční elektronová paramagnetická rezonance (HF-EPR) rozmach v chemii, biologii, materiálových vědách a fyzice. Přesto jsou HF-EPR spektrometry pracující na frekvencích blížící se THz ve světě vzácné. Cílem této dizertační práce bylo vyvinout nový širokopásmový EPR spektrometr schopný pracovat jak v širokém magnetickém poli tak v široké frekvenční oblasti a který by byl schopen provádět rychlé skenování frekvencí pro studium relaxačních časů. Vyvinutý spektrometr pracuje při magnetických polích 0-16 T, frekvenční rozsah od 90 do 1100 GHz a teplotní rozsahy 4 – 400 K. V práci je dále popsán návrh a vývoj šesti různých výměnných držáků vzorků s EPR měřeními, které prokázali jejich funkčnosti. Design obsahuje navíc unikátní rychloupínací přírubou pro rychlou výměnu vzorku společně s držákem vzorku. Schopnost spektrometru provádět rychlé skenování frekvence pro měření relaxačních časů je demonstrována na měření LiPc monokrystalu a vzorku DPPH rozpuštěného v toluenu.

KLÍČOVÁ SLOVA

Elektronová paramagnetická rezonance, elektronová spinová rezonance, EPR, ESR, vysoké frekvence/pole, HF-EPR, rychlé skenování, držák vzorku pro EPR

Author's Declaration

Author:	Ing. Antonín Sojka
Author's ID:	151669
Paper type:	Doctoral thesis
Academic year:	2022/23
Topic:	Development of a Novel Terahertz Magnetic Resonance Spectrometer for Spin Dynamics Investigations

I declare that I have written this paper independently, under the guidance of the advisor and using exclusively the technical references and other sources of information cited in the paper and listed in the comprehensive bibliography at the end of the paper.

As the author, I furthermore declare that, with respect to the creation of this paper, I have not infringed any copyright or violated anyone's personal and/or ownership rights. In this context, I am fully aware of the consequences of breaking Regulation § 11 of the Copyright Act No. 121/2000 Coll. of the Czech Republic, as amended, and of any breach of rights related to intellectual property or introduced within amendments to relevant Acts such as the Intellectual Property Act or the Criminal Code, Act No. 40/2009 Coll. of the Czech Republic, Section 2, Head VI, Part 4.

Brno ....

author's signature*

*The author signs only in the printed version.

ACKNOWLEDGEMENT

I want to thank everyone who contributed to creating this work on this page. First, I have to thank all students I was supervising or co-supervising. Here, I want to thank them for their fantastic work: Ing. Tomáš Martinek for the first concept of Fast loading mechanism [1], Bc Adam Lagin for the design of Chip Sample Holder Carusel sample Holder [2], Bc Andrej Gabris for design Rotator Sample Holder [3], Bc Tomáš Fargač for the first version of the program for automatic coupling [4], Ing Tomáš Láznička for design Vacuum Sample Holder [5].

Next, I want to thank all members of the CEITEC MOTeS group, as I found many great friends who helped me answer scientific questions and move forward in my professional life. I would like especially thanks to this members: Doc. Ing. Petr Neugebauer, Ph.D. for supervising me and for allowing me to work on this project and for all advice and help which he gave me during my PhD., Dr. Vinicius Tadeu Santana for co-supervising me, helping me to understand the theory of EPR, teaching me the simulation of EPR spectra, and for help to write this work, Dr. Oleksii Laguta for co-supervising me, and all advice which he gave me during the design and troubleshooting of EPR and rapid scan measurement, Ing. Matúš Sedivý for his software contribution, Mgr. Luboš Havlíček for all samples he prepared, Ing. Jakub Hrubý for many advices and English corrections.

Furthermore, I would like to thank professor Olivier Oari, professor Mark Sherwin, professor Graham Smith, and professor Joris Van Slageren for internship in their groups where I learn a lot about the EPR. Next, I would like to thank people from CEITEC BUT, especially the CEITEC NANO facility and Dominik Varga from the CEITEC NANO workshop. Then, I thank Ladislav Křenek and Josef Píša for collaborating on EPR spectrometer cover plates. And last but not least, I would like to thank all my friends, the members of HOV* group, Tomáš, Filip, and my family for the big support and the nice distraction from time to time. In the end, I want to thank my wife Anetka for all her support, advice, and sometimes strong kick to keep me focused and help me finish this P.hD.

At the end I would like to acknowledge the projects financing my Ph.D. study and research: mainly to ERC (GA No. 714850) with the topic THz Frequency Rapid Scan – Electron Spin Resonance spectroscopy for spin dynamics investigations of bulk and surface materials, CZ-USA Inter-Excellence with topic Spectroscopy of single molecular magnets using graphene bolometers, Internal CEITEC project for creating a new education course with the topic Laboratory courses in Electron Paramagnetic Resonance, COST+ with the topic Influence of Substrates on Magnetic Properties of Deposited Single-Molecule Magnets.

Contents

Introduction

Spectroscopy is one of the keystones in our understanding of nature and the development of new technologies. Generally, spectroscopic methods are based on the energy exchange between electromagnetic waves and a sample, where the oscillating electric field component of the wave (E_1) interacts with a studied material, as in Optical Microscopy (OM) and others. In the cases of Electron Paramagnetic Resonance (EPR) and Nuclear Magnetic Resonance (NMR) spectroscopies, the oscillating magnetic field component (B_1) plays a dominant role in the interaction with the samples.

Both methods are very similar to each other. While in NMR, the electromagnetic wave interacts with nuclei, in EPR, it interacts with the spin of an electron. The techniques are based on the Zeeman effect, the electromagnetic wave's interaction with the spin of nuclei or electrons in a magnetic field. The difference in the required energy in EPR and NMR leads to a different range of frequencies that the spins need for excitation. Electron spins require three orders of magnitude higher energy to be excited than nuclei spins. The resonance condition implies that the irradiation frequency ratio to the magnetic field scales as 28 GHz/T in EPR and 42.5 MHz/T in NMR, comprising the microwave (m.w.) and radio frequency range. The requirement of higher energies led to slower development of EPR due to technical challenges, making NMR spectroscopy still more popular nowadays.

Since its discovery in 1944 by Zavoisky [6] and parallel to the progress in the technology of m.w. propagation, m.w. sources, m.w. detectors, and superconducting magnets, EPR has been a thriving technique. Its popularity still grows as the energy range covered by this spectroscopic method moves to high frequencies and fields (HF-EPR) (above 120 GHz and 4.3 T) [7], providing more information about the sample, higher sensitivity and resolution. Nowadays, applications of HF-EPR can be found across many scientific disciplines. For example, biologists use EPR for the calculation of distances between the atoms in proteins and molecules [8–10], chemists and physicists for determination of chemical structure and magnetic properties of molecules [11–14], and for magnetic studies of a wide range of system including monolayered materials [15, 16].

Goal of the thesis and Motivation: The interaction among spins and their environment can be described by the spin-lattice (T_1) and spin-spin (T_2) relaxation times. The access to relaxation times is crucial for the understanding and development of spin polarization agents in dynamic nuclear polarization (DNP) techniques [17, 18], and single-molecule magnets (SMMs) or single-ions magnets (SIMs) based quantum bits [19–23]. In this regard, EPR has access to relaxation times. Usually, such a

task can be accomplished by pulsed EPR spectroscopy. In this method, the sample is irradiated by a series of pulses that flip the magnetization. The relaxation of the magnetization to its origin occurs in a specific time scale that is detected according to a given sequence of pulses. However, pulsed EPR resolution depends on the power of m.w. source (1 kW and more), which is at high frequencies hard and expensive to accomplish. Moreover, HF-Pulsed-EPR has additional disadvantages imposed by the limited sample space due to the use of cavities (at 263 GHz samples are placed into a capillary with only 30 µm diameter), narrow operating band (only few GHz), and dead time which complicates measuring relaxation times bellow 50 ns [24]. These limitations can be overcome by a method called Rapid Scan EPR (RS-EPR) spectroscopy. In RS-EPR, the frequency or field is swept fast through the resonance. Suppose the sweep is comparable or faster than the relaxation time of the studied system. In that case, one can obtain an oscillatory signal called "wiggles" in the EPR spectrum, which contains information about T_2 relaxation time.

The frequency-domain rapid scan measurements are more complicated to accomplish as they require a fast sweeping frequency source. Therefore, most of the published results employ field domain rapid scan [25, 26], which is easier to realize by adding sweeping coils around the sample. However, the measured band is narrow (hundreds of mT). Moreover, the data acquisition in RS is extremely fast, ms or faster, which gives the possibility to study fast processes, and additionally, RS can gain sensitivity of spectrometer under certain conditions [27]. Nevertheless, the advantages of frequency-domain rapid scan are significant, and as the progress in technologies bring more power, broader range, and more stable m.w. sources, a wider range of opportunities will be available for applying this method. In 2018, Oleksii Laguta with Petr Neugebauer showed the advantages of broad frequency rapid scan [28]; no dead time, access to ns relaxation times, and possibility to acquire T_2 relaxation time at any frequency within the range of the spectrometer. They also pointed out the problems of a rapid scan, standing wave, and significant background, which can bury the RS signal.

The main goal of this Ph.D. thesis was to design, build, and troubleshoot a novel resonance-free high-frequency/high-field EPR spectrometer that is able to operate at the same time in a frequency and field domain, and advance the frequency-domain rapid scan technique at high frequencies. Specifically, by performing frequency rapid scans on radicals dissolved in liquid that will impact on the future of Dynamic Nuclear Polarization (DNP) applications [29]. The successful study of such radicals in high magnetic fields is a necessary step in understanding and optimizing the nuclear polarization efficiency and developing spin polarization agents. The importance of DNP in Nuclear Magnetic Resonance (NMR) lies in a significant enhancement, up to several orders of magnitude, of NMR signals [17, 30–32].

1 Theory of EPR

The basic principle of EPR is based on the Zeeman effect (Fig. 1.1), where the oscillating component, B_1, of an electromagnetic wave at frequency f interacts with the magnetic moment of an unpaired electron spin, $S = 1/2$, in the presence of an applied external magnetic field B_0. The resonance condition for $S = 1/2$ is then as follows:

$$\Delta E = E_u - E_l = hf = g\mu_B B_{res}, \tag{1.1}$$

where E_u and E_l are the energies of the two possible m_s states of spin $S = 1/2$, B_{res} is the resonance field.

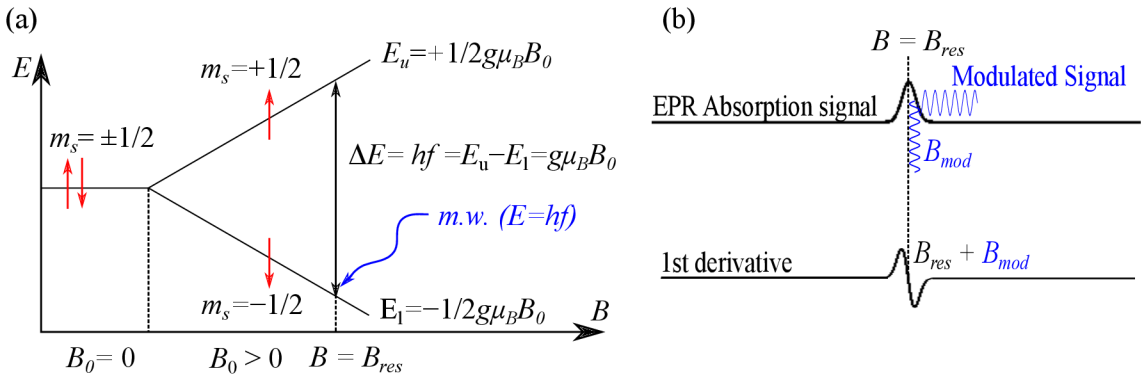

Fig. 1.1: Example of the interaction between a hydrogen atom with spin 1/2 and the external magnetic field. If the amplitude of external magnetic field B equals to zero, there will be no energy difference between the spin state $m_s = +1/2$ and $m_s = -1/2$. However, if the external magnetic field has a non-zero value, the separation between the energy states occurs. By applying an external electromagnetic wave with energy equal to the separation of the energy states, the spin can be excited to the higher state.

The resonance condition implies that irradiation frequency scales by 28 GHz/T, m.w. range. An absorption EPR signal is observed when the resonance condition is fulfilled, *e.g.* when the electromagnetic wave's energy hf matches the energy levels' separation ΔE (see Fig 1.1). In order to further improve EPR signal-to-noise ratio (SNR), a small modulating field, B_{mod}, oscillating at few kHz, is applied, leading to the actual measurement of the derivative of an absorption spectra (Fig. 1.1, right) [33]. In the case of a system with more than one unpaired electron, $S > 1/2$, the spin-spin and spin-orbit couplings may lift the degeneracy of spin states even at zero-field, the so-called zero-field splitting (ZFS).

Nevertheless, other physical phenomena play a role in spin systems. For many relevant applications, those phenomena lies in the range of higher energies and require higher magnetic fields and frequencies to be adequately detected and described. Therefore, Hamiltonian contains these terms:

$$H = H_{Zeeman} + H_N + H_{HFS} + H_{LS} + H_{elect} + H_{ef} + H_{SS} + H_Q, \qquad (1.2)$$

where new components represent the following interactions:

H_{Zeeman}	Electron Zeeman energy
H_N	Nuclear Zeeman energy
H_{HFS}	Hyperfine structure
H_{LS}	Spin - orbit interaction
H_{elect}	Electron repulsion energy
H_{ef}	Crystal (ligand) field energy
H_{SS}	Spin-spin interaction
H_Q	Nuclear Quadrupole energy

1.1 Frequency domain vs Field Domain EPR

There are two ways to meet the resonance conditions in an EPR experiment. The sample can be either irradiated by a m.w. beam with constant frequency during sweeping of the magnetic field (Magnetic Domain Magnetic Resonance (MDMR)) or to maintain a static magnetic field and sweep the frequency of the m.w. radiation (Frequency Domain Magnetic Resonance (FDMR)). Irradiating the sample at the constant frequency during the experiment is called continuous wave- EPR (cw-EPR).

In many samples, the study energy splittings are caused by field independent interactions, such as zero-field splitting (ZFS) or crystal-field splitting. An FDMR measurement has a significant advantage over the MDMR in that the EPR spectrum is recorded even at zero fields [34]. Therefore, the energy spectrum of the study system is recorded directly, while in MDMR, those properties have to be extrapolated. Moreover, to determine magnetic parameters by EPR precisely very often are required a multifrequency study [35]. Typically, these studies are presented as frequency filed plots [36]. In MDMR, the HFEPR spectrum is often recorded as a series of different frequencies, which is extremely time-consuming because the ramp speed of the superconducting magnet is defined by the capacity of the cryogenic system [37]. Therefore, it is beneficial to record FDMR spectra together with continuous ramping of the magnetic field. The result, *EPR map*, is a two-dimensional frequency-field map. Moreover, FDMR achieves a much faster sweeping time that

could be hungered of GHz in milliseconds or even faster in the so-called rapid scan regime (discussed in section 2.4.). In comparison sweep rate of MDMR, limited by the cooling power of its cryogenic system, results in T per minute with superconducting magnets [38]. Additionally, the FDMR spectrum can be recorded even while the magnet is in persistent mode to save the valuable resource of liquid helium. Lastly, some of the samples have an energy spectrum that spans over a broad energy range up to several THz [39]. In such cases, magnetic fields required to measure MDMR are impossible to achieve.

1.2 Advantages of EPR in High Fields/Frequencies

Increasing sensitivity: Another advantage of using high frequencies is the increase in detection sensitivity. The ratio between the Boltzmann distribution of the population of the spin states in a two-level system in equilibrium by applying a magnetic field, as it is the case for a $S = 1/2$ system is given by

$$\frac{N_u}{N_l} = \exp\left(-\frac{E_u - E_l}{kT}\right) = \exp\left(-\frac{hf}{kT}\right), \tag{1.3}$$

where E_u and E_l are the energy corresponding to the $m_s = 1/2$ and $m_s = -1/2$, N_u is the number of spins occupying the higher energy level, and N_l is the number of spins occupying the lower energy level, k is the Boltzmann's constant, and T is thermodynamic temperature.

Higher spectral resolution: A variety of the sample [8]: molecules with g-anisotropy (molecule orbital orientation to the magnetic field is represented as g_x, g_y, g_z), samples containing two systems with slightly different g-factor, or systems containing hyperfine splitting are studied in high magnetic fields and frequencies, where those species are well separated (see Fig. 1.2).

Zero-field splitting detection: For $S > 1/2$, the so-called high-spin systems, the zero-field splitting (ZFS) term H_{ZFS} in equation 1.2 plays a fundamental role [42, 43]. To see ZFS by EPR experiment directly, it is typically necessary to use high m.w. frequencies that correspond to the separation between the energy levels [44, 45]. Spectrometers operating at lower frequencies (X-band, Q-band, W-band) are not suitable for the studies of molecules with high ZFS, which are referred in the literature as "EPR silent". The strict meaning of "silent" is therefore connected to the availability of a suitable spectrometer to probe the transitions in the studied material.

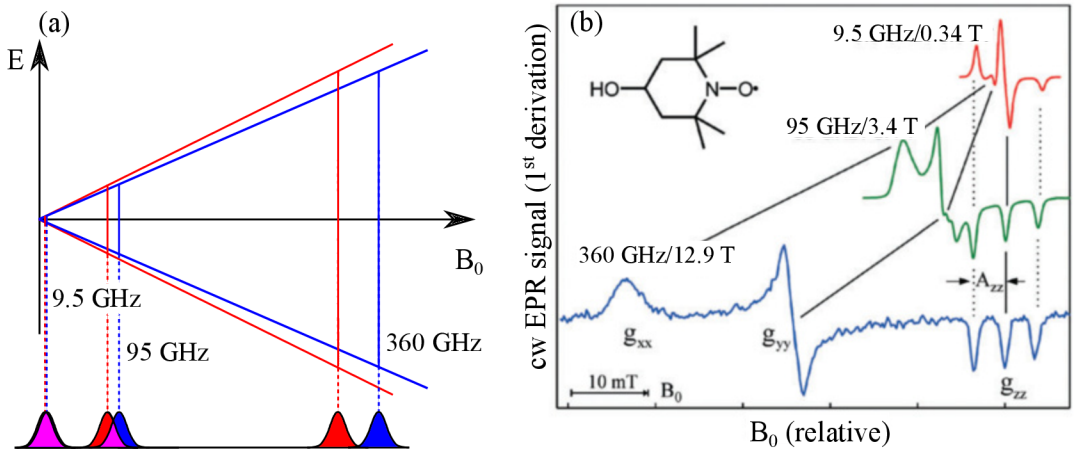

Fig. 1.2: a) Two species of different g-values are very diffcult to distinguish at the X-band (9.5 Ghz) frequency. The situation gets better for the W-band (95 Ghz) frequency where we can already see the two lines presented. However, only the lines for the high (360 Ghz) frequency are fully separated. The resolution of a W-band spectrometer can be considered as one order of magnitude higher than that of a X-band spectrometer. Taken from [40]. b) First-derivative CW-EPR spectra of a TEMPOL in frozen water solution at different microwave frequency/B_0 settings. The spectra are plotted relative to the fixed g_{zz} value. Taken from [41].

1.3 Rapid Scan

CW-EPR has many advantages and applications, but it gives limited and mostly indirect information about magnetic relaxation and spin dynamics [46], which plays an important role in the field of dynamic polarization [17, 18, 47] and quantum computation [19,48]. Generally, to get information about spin dynamics pulsed EPR is used [49–52]. In pulsed EPR, by irradiating the sample with a series of short m.w. pulses, an echo is created as a response from magnetization. Echo measurements can provide T_1 spin-lattice relaxation times and T_2 spin-spin relaxation times [8]. However, pulsed EPR requires high power pulses, which require very expensive m.w. components. In the THz frequency range, such high power devices are solid-state sources [53] or high power klystrons, gyrotrons, and free-electron lasers [54], which besides being expensive are large, the tuning range is usually smaller than 2 GHz and therefore to cover the broader hundreds of GHz range is not possible. The alternative to the pulsed EPR starts to be Rapid Scan EPR. So far, there is only one working rapid scan spectrometer worldwide in frequency domain that operates below 95 GHz [55] and recently one in 170-250 GHz range [28]. In generall, pulsed and rapid scan EPR require less time to acquire spectra with comparable signal-

to-noise than conventional CW EPR. The comparison between Pulsed EPR, Rapid Scan EPR and Cw-EPR can be found in [56].

Rapid Scan Theory In this method, either the frequency or magnetic field is swept through the resonance faster than the sample's spin relaxation time. The fast sweep rate influences the line shape, creating "wiggles" (RS signal), which allows the determination of the spin dynamics. In RS is not possible to measure T_1 relaxation, but it measure T_2* relaxation [57]. Then, the relaxation time T_2 can be obtained by fitting the signal with the modified Bloch equations [15, 58]. The deconvolution of the RS signal removes "wiggles" giving a non-distorted EPR absorption spectrum.

Modified Bloch equation: Bloch equation were introduced in the section 2.3.2, with their steady state solution. The steady solution describes the slow passage through the resonance to observe an absorption. In RS-EPR, the fast passage through resonance is applied, which allows for observation of relaxation effects ("wiggles"). The main condition to observe wiggles is that passage (of frequency f or field B_0) has to be faster than the relaxation time of the system:

$$\gamma \left| \frac{dB_{ext}}{dt} \right|, \left| \frac{df}{dt} \right| \geq \frac{1}{T_2^2}. \tag{1.4}$$

The RS wiggles are the result of the beating process of two oscillations: B_1 excitation via microwave oscillation (in field domain, it is the oscillation of magnetic field B_0) and magnetization oscillation of the spin system. The number of wiggles is proportional to the difference in the frequencies of the two oscillations. The rapid scan signal $r(t)$ is described as convolution of slow-scan signal $s(t)$ and drive function of the excitation $d(t)$:

$$r(t) = (s * d)(t) = \int_{-\infty}^{+\infty} s(\tau) d(t - \tau) d\tau. \tag{1.5}$$

The solution to the equation through convolution is complex. However, applying the Fourier transformation, the convolution operator is transformed to the multiplication operator, thus equation 1.5 becomes:

$$R(\omega) = S(\omega) D(\omega), \tag{1.6}$$

where $R(\omega)$, $S(\omega)$ and $D(\omega)$ are operators $r(t)$,$s(t)$ and $d(t)$ in Fourier space ($t \rightarrow \omega$). In this form can be calculated driven function easily, because it depends on experimental setup:. Generally, the drive function is:

$$d(t) = \exp\left(\int_0^t \omega(\tau) d\tau \right), \tag{1.7}$$

where $\omega(\tau)$ is the waveform of the sweep. If the sweep is linear then: $\omega = b\tau$, b is the sweep rate in rad/s^2 results into

$$d(t) = \exp\left(\frac{ibt^2}{2}\right) \Rightarrow D(\omega) = \exp(-i\omega^2/2b). \tag{1.8}$$

If the sweep is broad enough comparable to signal, sweep as sine waveform can be approximated by a linear function. Then the b is equals to the maximum sweep rate ($2\pi A_{mod} \times f_{mod}$, A_{mod} is modulation's amplitude and f_{mod} modulation frequency) occurring in the center of sinusoidal scan. Then, for obtaining the relaxation time T_2 it is necessary to simulate rapid scan spectra by solving a modified system of Bloch equations [28, 59–61]:

$$\frac{dM_x}{dt} = -\frac{M_u}{T_2} - [\Delta\omega + A_{mod}\cos(2\pi f_{Mod}t)]M_v, \tag{1.9a}$$

$$\frac{dM_v}{dt} = -\frac{M_v}{T_2} + [\Delta\omega + A_{mod}\cos(2\pi f_{Mod}t)]M_u - \gamma B_1 M_z, \tag{1.9b}$$

$$\frac{dM_z}{dt} = \frac{M}{T_1} + \gamma B_1 M_y - \frac{M_z}{T_1}, \tag{1.9c}$$

where $\Delta\omega$ is offset of a spectrum from the center of the sweep, M_u,M_v, and M_z are projection of the total magnetization M. The example of measured freqeuncy domain RS signal with the simulation is shown in Fig.1.3.

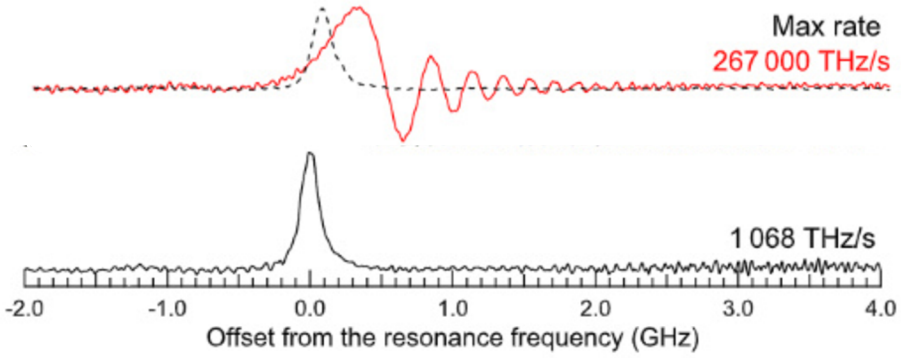

Fig. 1.3: Rapid scan spectra of the LiPc sample recorded at the fixed field of 8 T, temperature of 13 K and modulation frequencies 20 kHz and 5 MHz, and constant modulation amplitude of 8.5 GHz. In the first spectra, black, the sweep rate is not fast enough, and only absorption signal without "wiggles" is measured. Traces are labeled by the maximum sweep rate achieved at the center of sweep. Dashed curves are the deconvoluted spectra. Taken and adjusted from [28].

2 HF-EPR instrumentation

There are five general requirements for a cw-EPR spectrometer [62]: 1) The magnetic field has to be stable and homogeneous. 2) the m.w. source has to have enough power, produce a low level of noise, and a stable m.w. phase as well. 3) The m.w. propagation solution should have low m.w. power losses. 4) The sample holder must concentrate the incident m.w. radiation onto the sample, allowing detection of the small amount of energy absorbed or emitted when the EPR resonance condition is met. 5) The detector should have low noise floor to enable a high signal-to-noise ratio (SNR).

HF-EPR spectrometer: The schematic drawings of the cw-HF-EPR spectrometer with homodyne or heterodyne detection scheme is shown in Figure 2.1.

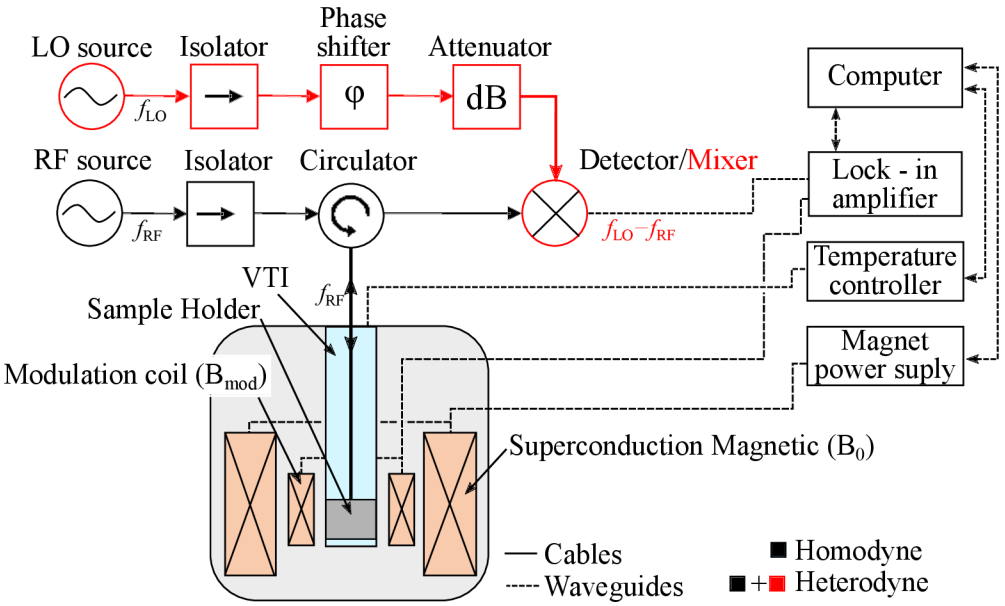

Fig. 2.1: The scheme of cw-HF-EPR spectrometers with heterodyne or homodyne detection.

Conventional homodyne cw-EPR employs a continuous microwave source (RF source) to irradiate samples located in the sample holder, which is placed inside a magnet cryostat. The m.w. is generated by RF source (part of the RF sources are often multipliers which upconverting generated frequency), and propagates to the sample through a circulator. Circulator is a passive device with three or four ports that allows a m.w. to exit through the port next to the one it entered. It protects the sensitive m.w. sources to be damaged from back-reflected m.w.. The mirror located under the sample reflect m.w. back to circulator and to the

mixer (heterodyne detection) or directly to the detector (homodyne detection (see Fig. 2.1). To increase the EPR signal, the m.w. passes through the sample two times (radiated m.w. from source and reflected m.w. from mirror), *double pass configuration*. For optimum sensitivity, the sample holder is exactly aligned to the transmission line waveguide in the way that all the incident m.w. power interacts with the sample. Furthermore, a small modulation coil is placed around the sample for SNR enhancement.

The more common EPR configuration is homodyne detection. Homodyne detection uses only one source and one detector. The advantage of homodyne setups is lower construction demands. The second configuration, heterodyne detection uses also a second source, *Local Oscilator* (LO Source), and mixer. The excitation m.w. (from RF source) carrying EPR signal with the signal from the local oscillator source (LO) are mixed, which resulting intermediate signal (IF) is produced. Systems with heterodyne detection have more components and thus are more complicated to build and optimize. On the other hand, they should theoretically achieve higher sensitivity than a system with homodyne detection, because of lower noise level and downconverting m.w. frequencies to lower frequencies, where low noise amplifier and filters are available [62].

HF – EPR transmitting system In HF-EPR development, the low-loss transmitting system is critical. A low-loss m.w. transfer system, which operates in a broad frequency range, has been one of the aims of EPR development for decades. In X-band spectrometer (9.6 GHz), the transmission line is made of rectangular waveguide WR90, which attenuates the power by 0.1 dB/m. For a typical X-band transmission line length of 1 m such loss does not disturb the outcomes significantly. However, at high m.w. frequencies, a transmission lines are generally longer, and losses in standard rectangular lines are higher. For example in our case, the pathway distance source to the detector is around 3 m. At 140 GHz the rectangular waveguide WR7 attenuates by 5.6 dB/m at room temperature [62]. One of the general solutions for a low loss system is to used an oversized waveguide [63]. Therefore, Gaussian Quasi-Optical (QO) approach is often used in the design of HF-EPR spectrometers.

Since the late 1980s, several groups have begun replacing waveguides in their HF-EPR systems with a more efficient quasioptical system for microwave propagation which soon become standard in HF-EPR spectrometers [35,54,64–66]. This method considers both ray-like and diffraction-causing optical phenomena when tracing the beams as they interact with the surfaces of optical elements and the matter in the pathway. The optimized m.w. transfer systems operating in free space can have negligible damping of dB/km (damping is mostly caused by molecular air absorption).

3 FRaSCAN EPR

This chapter describes the design and development of the sub-THz Frequency Rapid Scan (FRaSCAN) EPR spectrometer (see Fig. 3.1).

Tab. 3.1: Parameters of FRaSCAN EPR spectrometer:

Frequency Range	m.w. power	Magnetic Field	VTI Temperature
$(82 - 1100)$ GHz	$(100 - 0.003)$ mW	(0 ± 16) T	$(1.8 - 400)$ K

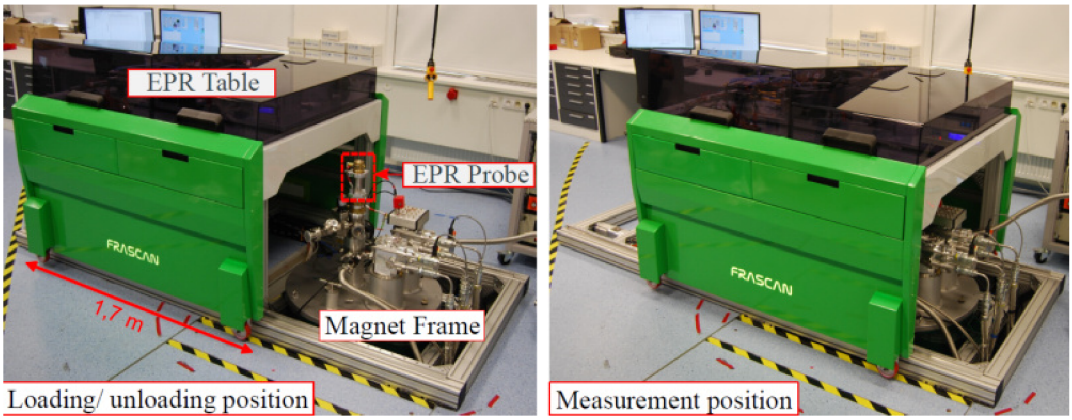

Fig. 3.1: The photograph of FRaSCAN EPR spectrometer in position for loading/unloading of the probe and measurement position. The picture was taken in June 2020.

Overall design: The FRaSCAN EPR spectrometer is spectrometer working in the induction mode, and with heterodyne detection. To perform the EPR measurement, firstly, the probe with a sample is inserted into the magnet. After that, the EPR table moves above the magnet into the measurement position where the m.w. beam from the EPR table is precisely coupled to the EPR probe (see Fig. 3.1). The main spectrometer specifications are listed in the table 3.1. It can work in the field domain with maximal constant ramp speed to 15.5 T is 3 mT/s, and in the frequency domain with sweep rate 14 ms/1 GHz (or 90 μs per 25 MHz for sweep over less than 50 MHz) simultaneously. Therefore, spectrometer is capable of measuring EPR maps, and HF-frequency domain rapid scan over a wide range.

The spectrometer has four main parts: Magnet Frame, EPR Table, EPR probe, and seven different sample holders shown in Fig. 3.2. All parts are standalone. The superconducting cryogen-free magnet is partially in the lab pit. The pit gives

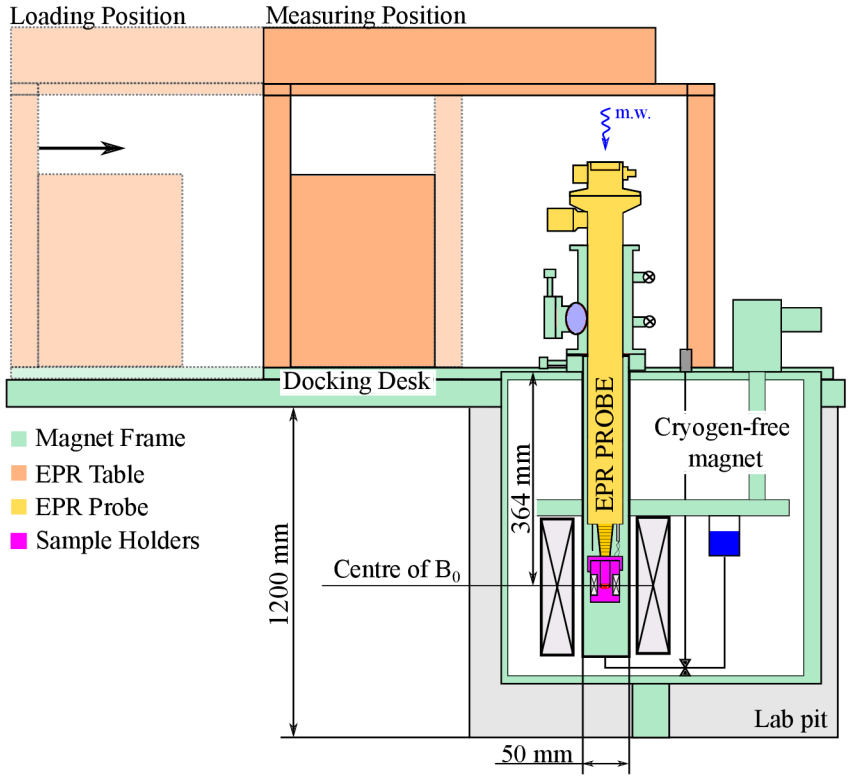

Fig. 3.2: Schematic drawing of the THz-FRaSCAN-EPR spectrometer. The spectrometer consists of a removable EPR table, magnet frame, EPR probe, and sample holder. After the probe is inserted into the magnet, the sample is located in the centre of the magnetic field. Then, the EPR table moves above the EPR probe to the Measuring Position, where the m.w. from the EPR table is coupled to the EPR probe, and the experiment can be performed.

space for Variable Temperature Insert (VTI) pump, and electronics, which would in another case, consume working space in our lab. The only equipments of magnet that is not placed in the lab are magnet compressors for the closed helium cryogenic system. They are installed in the cellar one floor below our lab to avoid their working noise in the laboratory.

The EPR table can be replaced with another movable setup allowing our magnet to be used with other techniques. The replacement was performed between the EPR table and FIR table, designed by Jana Dubnická Midlíková.

Methodology: All 3D models and drawings were done in Creo parametric (PTC Inc., USA). Some of the 3D models (holders of cables, shafts, holders for Faradaz Rotator, etc.) were 3D printed on 3D printer Delta M (TriLAB Group s.r.o., CZ) to reduce the final cost and speed the spectrometer development. All programs were

programmed in LabVIEW (National Instruments, USA).

3.1 Magnet Frame

The magnet frame (see Fig. 3.3) is mostly assembled from Aluminum profiles (Bosch Rexroth s.r.o., Germany). The main advantages of aluminum profiles over the welded assembly are the modularity and simple construction of the frame.

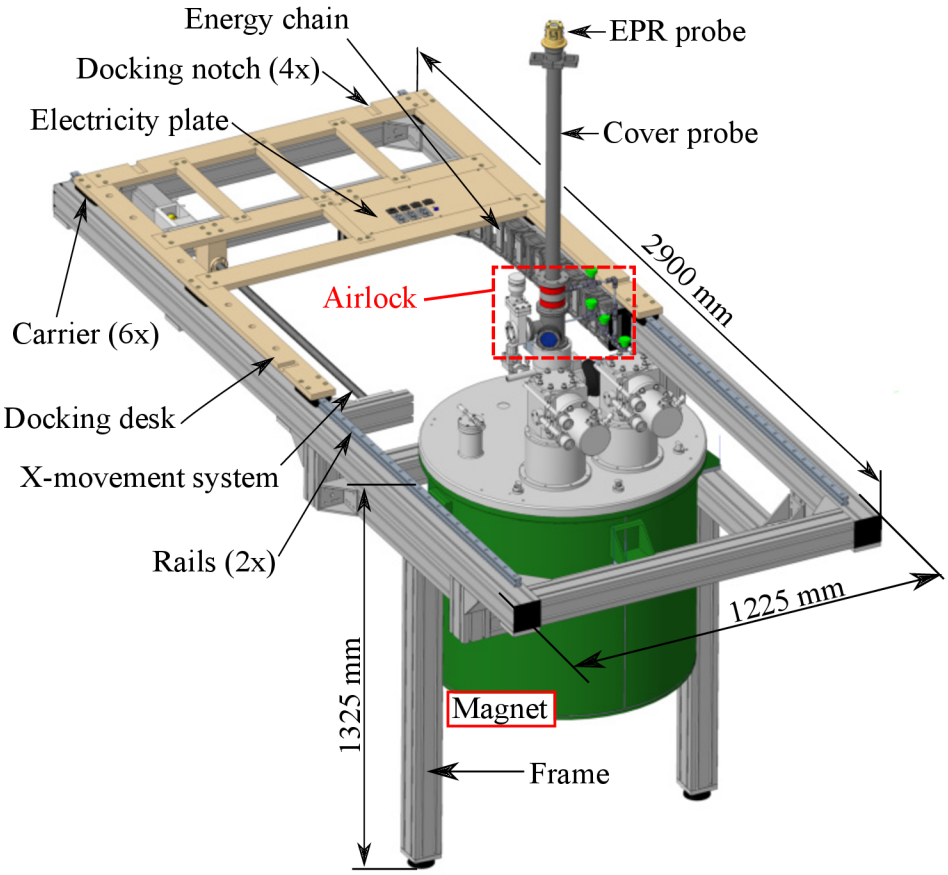

Fig. 3.3: 3D model of the magnet frame. The docking desk is in the loading/unloading position, while the EPR probe is inserted inside the airlock.

The parts of the magnet frame are the superconducting cryogen-free magnet, airlock, docking desk with the servo-driven system (x-movement system). The superconducting magnet (Cryogenics Ltd., UK) is attached to the frame in a way that the airlock inserting bore is in the user-friendly height of 512 mm. It is a cryogen-free magnet. The most significant advantage of such a system is that it does not need refilling liquid helium and nitrogen. It has some disadvantages, such as the limited cooling power that limits the possible sweeping rates of the magnetic field

(mT/s) and maintenance of the cooling system, during which the system has to be warm up for several days.

The magnet cryostat, VTI, allows to control the temperature in the sample space from 1.8 K to 400 K by circulating He gas in a separate circuit. However, it also requires special handling with loading a sample, namely when inserting and removing the probe, because the circuit is prone to blockage caused by air contamination. Therefore part of the magnet frame is a home-made loading airlock mechanism mounted on the top of the magnet (see Fig.3.3 and Fig. 3.4). The airlock is equipped by a port for side-loading air-sensitive samples with an optical window to check the sample in sample holders visually.

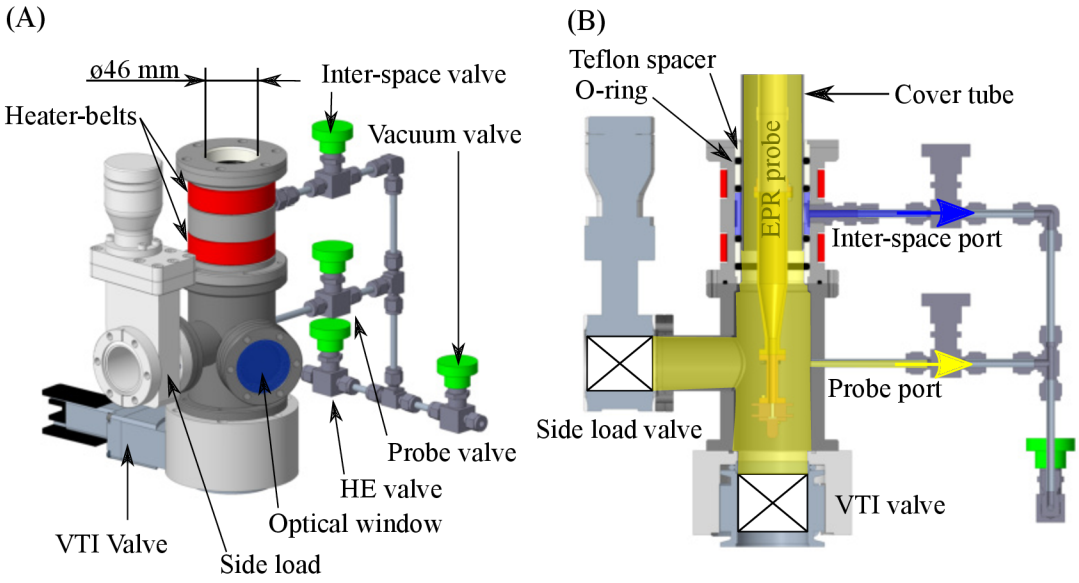

Fig. 3.4: A) The 3D model of Airlock. B) Cut view of the airlock with loaded EPR probe.

To insert the EPR probe into the VTI, the probe has to be loaded into the airlock first with the VTI valve closed. When the probe is loaded into the airlock (see Fig. 3.4), the operator opens the inter-space, probe, and vacuum valves connected to the scroll pump. Air from the airlock and the EPR probe (waveguide, sample holder, etc.) is pumped out by the airlock's probe port. The inter-space port serves for pumping the space between the o-rings. He-valve is used to flash the probe and airlock with He gas to reach a better vacuum level. When the vacuum inside the EPR probe reaches a sufficient level, the operator closes the probe port. Then, the VTI valve is opened, the EPR probe is slowly inserted into the magnet. Since the inter-space port remains open, any air that would pass the first two o-rings will be pumped out, and the He gas inside VTI will not be contaminated, a procedure known as differential pumping.

3.1.1 Vacuum transfer system

Part of the EPR table design was the system for transferring the air-sensitive sample from the UHV chambers (see Fig. 3.5). The main reason for the custom-made vacuum case was more flexible and broad compatibility not only with our EPR Table and the cost.

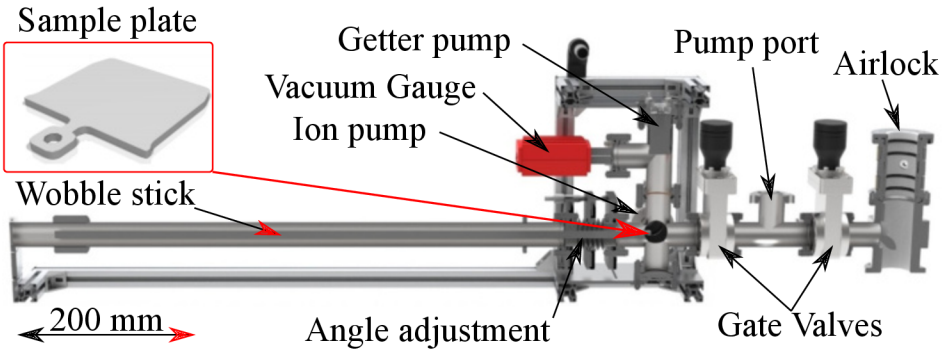

Fig. 3.5: Design for the EPR transmission system connected to airlock system (without supporting frame) for loading samples into EPR magnet.

The test transfer between the magnet frame and UHV complex was tested with a copper crystal mounted in an omicron plate. The vacuum pressure, in that case, was during the transfer $5.7 \cdot 10^{-9}$ mbar with a drop to 10^{-6} during the loading of the sample into the airlock. The transfer test monitored the level of copper sample contamination during the transport. The contamination levels of nitrogen, oxygen, and carbon elements, the main polluting elements, were measured before and after the transfer. XPS spectra were acquired and compared with the XPS spectra before transportation, resulting in a minor carbon contamination.

3.2 EPR Table

The main parts of EPR table are the aluminum frame (similar to magnet frame), EPR bridge for m.w. manipulation (QO), m.w. sources, and m.w. detectors), and electronics for EPR experiments. The EPR bridge is covered by two removable plexiglass covers to protect QO components from mechanical damage and dust (Fig. 3.6). Some of the QO components like the Faraday rotator and corrugated waveguides/horns of sources and detectors operate only in a certain frequency range and need to be replaced for each frequency band. Therefore, the plexiglass cover is split into two halves to be easily taken down for QO components replacement.

To easily undock or dock the EPR table from the magnet frame, the table has four retractable legs and four docking pins. The coupling of the m.w. between the

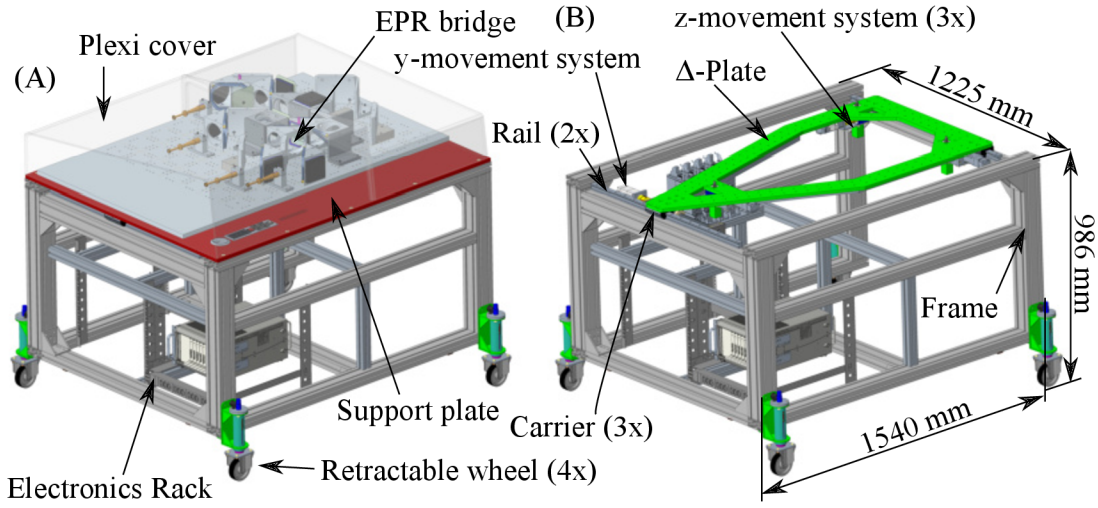

Fig. 3.6: The 3D model of EPR table. A) The model displays the EPR bridge covered by plexiglass covers. B) The model without EPR bridge, plexiglass covers and support plate.

EPR probe and EPR bridge is realized through an automatized coupling mechanism. The QO sits on pins of three z-movement systems mounted to the delta plate, which is screwed to the linear rails with the y-movement system connected. All controllers such as lock-in, digitizer, servo-electronics, source meter, and 9V/24V power sources are mounted in the electronic rack.

EPR Bridge The EPR bridge contains m.w. source, m.w. detector and QO solution with reasonably low m.w. attenuation. Most of the parts of the spectrometer are frequency-independent parts with low losses. However, some components are specific for a "narrow"-frequency range (100 GHz) and have to be replaced according to the desired operating frequency. Therefore, the nominal operating frequency range of the spectrometer - 82 to 1100 GHz - is divided into seven bands with different frequency ranges and powers (see Table 3.2). Mirrors, wire grids, and absorbers can be in our frequency range taken as frequency-independent components [63]. Faraday rotators, corrugated waveguides (EPR probes and antenna horns) connected to mixers and multipliers are frequency dependent. A unique detector and multiplier combination is also specific for each frequency range.

[1]Horns line specify the output size of waveguide for corresponding horn antennas.

[2]The multipliers are described according to the used AMC (9 or 12 multiplication) and the specific doubler x_2 or tripler x_3.

Tab. 3.2: The basic information about the separate frequency bands.

f(GHz)	82-125	110-170	170-280	250-350	350-500	500-750	750-1100
λ (mm)	3.6-2.4	2.7-1.8	1.8-1.1	1.2-0.9	0.9-0.6	0.9-0.4	0.4-0.3
Horns[1]	WR9.0	WR6.5	WR4.3	WR2.8	WR2.2	WR1.5	WR1.0
P(dBm)	+20	+17	+13	0	−3	−5	−25
P(mW)	100	50	20	1	0.5	0.32	0.003
Mult.[2]	9	12	9+x_2	9+x_3	12+x_3	9+x_{2+3}	12+x_{2+3}

In our setup, desired m.w. frequency is generated by a combination of multipliers fed by m.w. from AMC (Amplifier / Multiplier Chains) and synthesizers. The output frequency of synthesizers is still the same, 9.11 to 13.9 GHz. Therefore, more multiplication has to be used to achieve a higher frequency, which causes that source m.w. output power is smaller at higher bands. At highest frequency band, sources output power is 0.003 mW[3]. All m.w. sources, detectors, AMC and multipliers were bought from VDI (Virginia Diodes, Inc., USA).

A closer look at the Fig. 3.7 reveals two source lines, local oscillator (LO) and radio-frequency (RF), and three detectors, cross-polar mixer (XP), co-polar mixer (Co), and final mixer. The LO does not propagate to the sample. Instead, the polarizer splits the LO beam into two separate lines, propagating directly to the mixers. The RF m.w. propagates into the EPR probe (corrugated waveguide) and is reflected from the mirror under the sample. Then, the reflected RF beam at the output of the EPR probe can be split into two m.w. beams of the same frequency but different polarization. The m.w. beam whose polarization was changed by the sample is deflected by the polarizer above the probe and continues to the XP mixer. The unchanged m.w. beam goes through the polarizer and continues to the Co mixer. After the first stage mixing, the signal at the intermediate frequency (1800 MHz in our case) goes to the final mixer, where the signal is converted to the DC (m.w. from Co-mixer works as LO, here). In the first stage mixing. DC signal is then going into Lock-in *MFLI 500 kHz/5 MHz Lock-in Amplifier* (Zurich Instruments AG, CH), which is also feeding AC current into modulation coil. That helps to reduce the $1/f$–noise from the system's noise figure.

The spectrometer works in induction mode. The polarizer above the EPR probe reflects into the detector only m.w. beam containing information about the sample. The induction mode increases the sensitivity of the HF-EPR spectrometer by several orders. The principle is to detect only part of the signal which contains information about the sample. After passing of sample in resonance by linearly polarized beam,

[3]This power is smaller when it reaches the sample as it is attenuated during the propagation of m.w. through the QO system.

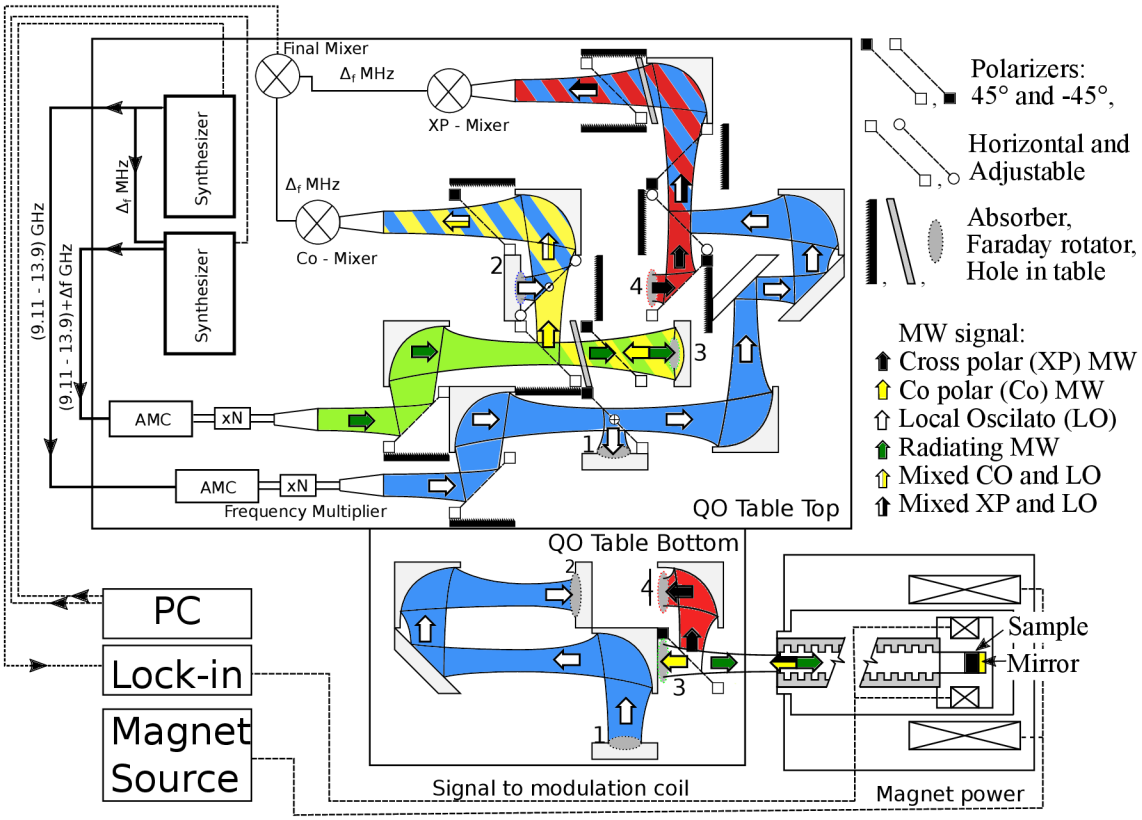

Fig. 3.7: Schematic drawing of QO solution of FRaSCAN. The legend describes the main symbols. The m.w. beam is generated in phase-coupled synthesizers multiplied by AMC and a set of multipliers (xN), depending on the required final frequency. The numbers in beam paths mark the holes in the QO where the beam propagates from table top to table bottom and vice versa.

the polarization will slightly change. The polarizer above the probe will deflect part of the m.w. beam with changed polarization into the XP line. Unchanged m.w. passes the polarizer and continue into the Co detector.

3.2.1 Automatized coupling adjustment

The FRaSCAN spectrometer was designed with a highly-precise servo-driven movement system. It is realized by five independent assemblies. The x-movement system driver is part of the magnet frame. It has the highest range of 1100 mm as it is used, except for precise position adjustment, to move docking desk (with the table docked) from the magnet when the probe is loaded into the magnet (see Fig. 3.8). The y-movement system is mounted on the Table frame and moves the Δ-plate perpendicularly to the x-movement system. The last three z-movement system are mounted on Δ-plate. They employ the gear that translates the rotary motion of the

servo into the linear motion of the pin. QO sits without a permanent connection on those pins. Therefore, the precise angle adjustment is realized by moving one of the three z-movement systems. If all three z-movement systems are moving at once, the height is adjusted.

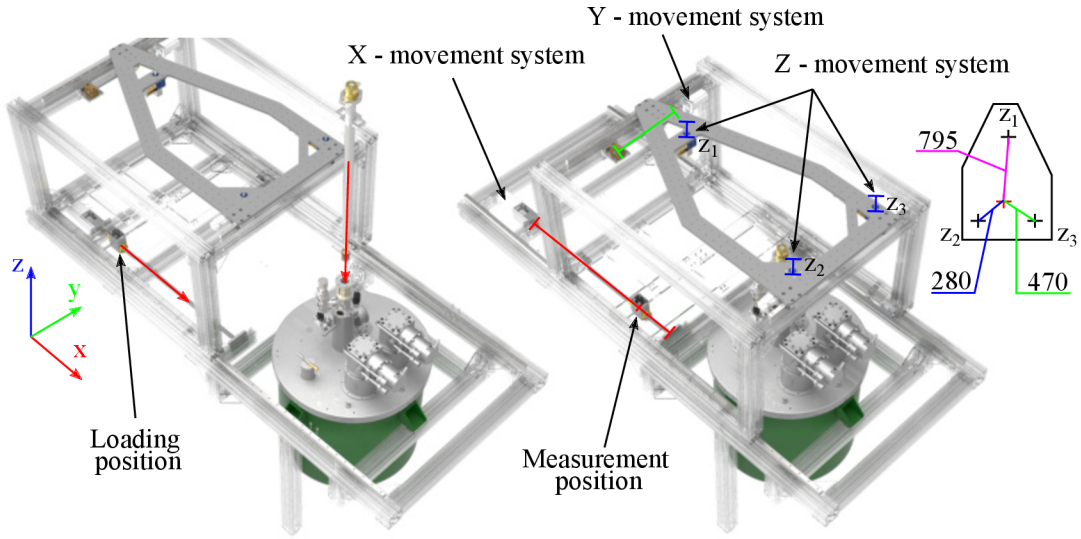

Fig. 3.8: Render of Coupling EPR Table with EPR probe via the servo-driven movement system. Left) the position of the table for loading the EPR probe into the magnet. Right) The position of the table at the measurements position. The x-movement and y-movement systems employ trapeze rods with driven and backslash nuts. The z-movement system is composed of three independent systems using a worm gearbox with a ratio of 4/1. The inset shows distances of z-movement systems from the m.w. output of the EPR bridge.

All servos are controlled manually via computer and software created in LabVIEW. The coupling adjustment is fully automatic. The operator has to find the signal in the frequency domain, and then it turns on the program, which will find the best position in several interactions. It shows that the software can find the position much faster than the operator in roughly 20 minutes. To compare, it took several hours to achieve the same results by adjusting the servos manually.

3.3 EPR probe

Fig. 3.3 depicts schematically the FRaSCAN EPR probe. The sample in a sample holder (SH) is at the end of a corrugated m.w. waveguide (Thomas Keating Ltd.,

UK), about 1 m long designed either for 430 GHz or 100 GHz made from German silver. The waveguide is placed inside a non-magnetic stainless steel cover (cover tube) and centered by sets of thermal shields along the waveguide. At the top of the probe, the m.w. corrugated waveguide is attached to the head, which contains 3 electrical connectors DBEE104A056, SFE104A086, SFE102A053 (Fischer Connectors, CHE) and one custom-built optical connector. The uniqueness of each connector prevents them from being changed unintentionally. The m.w. window in the head is replaceable. At the figure is shown a 2.213 mm-thick high density polyethylene (HDPE) film. The electrical wires (see Appendix) are shielded and guided in two stainless steel tubes to a fast loading flange (FLF), where the SHs are attached. The first tube carries wires for custom made modulation coils, temperature sensors (T-sensor) Cernox CX 1050 HT (LakeShore Cryotronics Inc., USA), and optional heaters and field sensors, the second tube guides wires for sensitive electrical measurements. Then, the m.w. is focused with EPR table through the HDPE window into the oversized corrugated waveguide with inner diameter 18 mm and propagates there with minimal losses to the inlet m.w. port of a SH using a focusing corrugated taper from 18 mm down to 5 mm diameter. The m.w. waveguide is used to guide also the reflected m.w. from a sample back to the outside optics. Furthermore, the cover tube is equipped with a port for a piezo step-motor (PiezoMotor Uppsala AB, SE) which is used to rotate a shaft used in CSH. The shaft goes down along the corrugated waveguide to the FLF. This motor can operate in a magnetic field and vacuum, but its functionality is uncertain at liquid helium temperatures. Therefore, the motor was placed in the upper part of the EPR probe, where the temperature is close to room temperature and hermetically sealed. Motion is then transferred to the sample platform by a perpendicular gear (1:1), approximately 90 cm long main shaft, a parallel gear (1:5), and a short second shaft that is inside a sample holder. Described mechanical parts are all made of brass to ensure the same temperature expansion and reduce stress (tension) that may evolve from room temperature down to cryogenic temperatures. In order to reduce temperature sinking through the main shaft, it was separated by

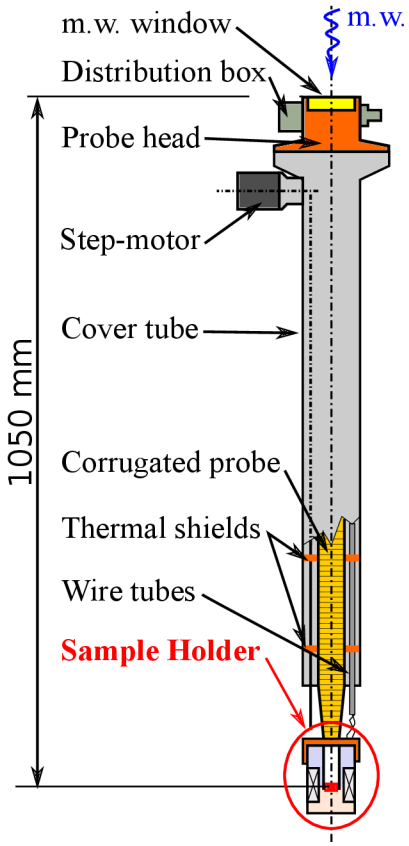

Fig. 3.9: Scheme of EPR probe.

two mechanical connectors, which were made of PEEK.

Fast Loading Flange (FLF) The design of the FLF consists of two main parts: a rotary and a base part (see Fig. 4.1). The rotary part is free to rotate in a given range on the base part and it has four grooves for the locking pins, one of which is larger to ensure a single coupling position for the SH. The base part is connected directly to the end of the corrugated waveguide. It has 24 female contacts CPINM-10 (LewVac, UK) divided into 3 connector blocks and a hole for a shaft connection. The rotary part rotates 90° around the axis of the waveguide, pushing the SH body and locking pins into the flange. Also upon rotation, all required contacts CPINM-10 are fastened to the female connectors grouped into three custom-made insulated 8-connector blocks. For good electric insulation and stability, the connector blocks are made from PEEK. The central 8-connector block contains electric contacts that are the same for all SHs: two for modulation coils, two for the T-sensor (Cernox CX 1050 HT, LakeShore Cryotronics Inc., USA), and four auxiliary ones can be used, for instance, for a magnetic field sensor (HGA-2302, LakeShore Cryotronics Inc., USA) or additional heater if needed. The other lateral 8-connectors blocks contain connectors for Rotator SH, Carousel SH and Chip SH (for more details see Appendix D.2). The rotary part of the flange is made from brass, whereas the base part from PEEK to provides thermal insulation of the SH from the corrugated waveguide resulting in better thermal control of the sample. Experimentally, we observe that this solution decreases the cooling time of the SH from 300 K to 4 K to six hours, which is 1/3 less of the time compared to the situation where the base part is made from brass.

Our probe is shielded by a stainless tube with an open bottom end, where the sample holder is mounted. The connection feedthroughs are placed on the top of the probe. The beam enters the probe through a thin Teflon or PET (Mylar) window, which is transparent for most of the EPR signal. Additionally, the probe is equipped with copper rings each having ø150 mm. These rings serve as temperature isolators, thanks to it the helium flow will be concentrated around the sample and not around the whole probe, i.e., the temperature gradient in the probe will decrease.

3.3.1 EPR probe features:

Attenuation of m.w. by EPR probe: TIn the test, we characterized only the 430 GHz probe with the flat mirror at the end. The average attenuation measured by the TK power meter is shown in the table 3.3.

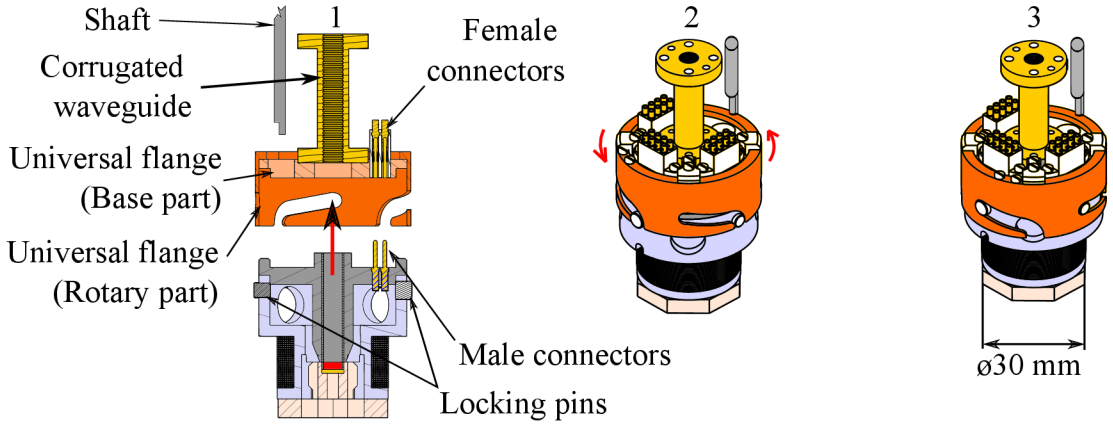

Fig. 3.10: 3D drawing of the FLM. 1) Orientation of the grooves of the universal flange (Rotary part) with the locking pins in sample holder, together with electrical connectors. 2) Rotation of the universal flange causing the full insertion of the male into the female connectors. 3) Locked position.

Tab. 3.3: The double pass attenuation of the probe measured by TK power meter.

Range (GHz)	80-125	170-250	240-380	320-500
Attenuation (dB)	3.7	2	2.71	1.6

Standing wave pattern: The standing wave patterns of three different windows were studied. The flat window manufactured from HDPE film has the highest intensity of standing wave patterns. The conical window from Teflon attenuates the m.w. by 4 dB compared to the flat mirror. A 30μm-thin PET (Mylar) film (typical food product packaging) can still hold a low vacuum inside the probe (needed due to airlock system loading) and is the best performance window.

The cooling performance: The cooling performance test was done with two slightly different setups. The difference between Setup 1 and 2 is the brass part of the FLF between the EPR probe and the sample holder (in setup 2 was removed), and an additional copper plate for the increasing flow of cold He through the sample in Setup 2. Due to this improvement (FLF made of peek and disk mounted at the bottom of the probe), the lowest possible temperature of the sample decreased from 6.5 K to 2.9 K. Furthermore, the time needed to cool down the selection dropped by more than half. The biggest improvement was uninstalling FLF and thus decreasing thermal flow from the corrugated waveguide. Therefore, we are using FLF made of PEEK in the current setup with an average time to cool down the sample of approximately 8 hours (time was measured from the loading procedure of EPR probe with PEEK FLF during regular operating of spectrometer).

4 Sample Holders

This chapter sum of the accepted paper to the journal IEEE named: *Sample Holders for Sub-THz Electron Spin Resonance Spectroscopy* [67]. Reproducible, fast and user-friendly exchange of SHs is very desirable for any measurement system, not only to HF-EPR spectroscopy. It speeds up the setting of a typical experiment, prevents user errors, i.e. a bad wiring or misalignment, which may affect reproducibility of the experiment and waste expensive measurement time. For that reason, we developed a set of SHs compatible with the FLF (see Fig. 4.1). All parts of the SHs need to withstand an operating temperature between 4 – 400 K with negligible volume changes to keep the m.w. alignment and thus to ensure good m.w. coupling with the sample. Additionally, they have to be non-magnetic and preferably non-metallic. For these reasons we found PEEK to be an optimal material, and most parts of the SHs are fabricated with it.

The design of different SHs can be split into two main categories: bottom-load and side-load SHs. The bottom-load SHs are easier to manufacture thanks to their cylindrical symmetry, have a modulation coil of a solenoid shape and provide an optimal m.w. alignment during the screwing of the functional part into the body. The side-load SHs possess an extra level of complexity that allows insertion via a side-load port of the airlock in case of air-sensitive samples or allow inserting multiple samples which can be loaded at once into the VTI, and use Helmholtz modulation coils. Both category are designed to have maximal outer diameter of 42 mm and can be split into three parts (Fig. 4.1): A) the Fast Loading Flange (FLF) that redistributes all the necessary contacts and is attached to the end of the corrugated waveguide; B) a body docked by four aluminium pins to the FLF with electrical connectors, and that contains a modulation coil and a smooth-wall m.w. waveguide; C) a functional part that contains the sample and is inserted into the body. All parts are described in the following text with greater details with demonstration measurements.

Body of sample holders: The body of SHs are made of PEEK with four aluminium pins to fit into FLF groves and several holes to allow effective Helium cooling. The body contain a modulation coil, smoth walled m.w. waveguide and a connectors part. As mentioned, we divide the SHs for bottom and side loaded, with solenoid or Helmholtz modulation coils, respectively. The precise field modulation amplitude was measured experimentally by overmodulating the EPR spectrum on a reference sample Lithium Phthalocyanine (LiPc). Obtained current values to create of 1 Gauss modulation at 1 kHz frequency are listed at the bottom of Fig. 4.1 including the type of coil and number of turns, wide from Cu 32 AWG wire (LakeShore Cryotronics

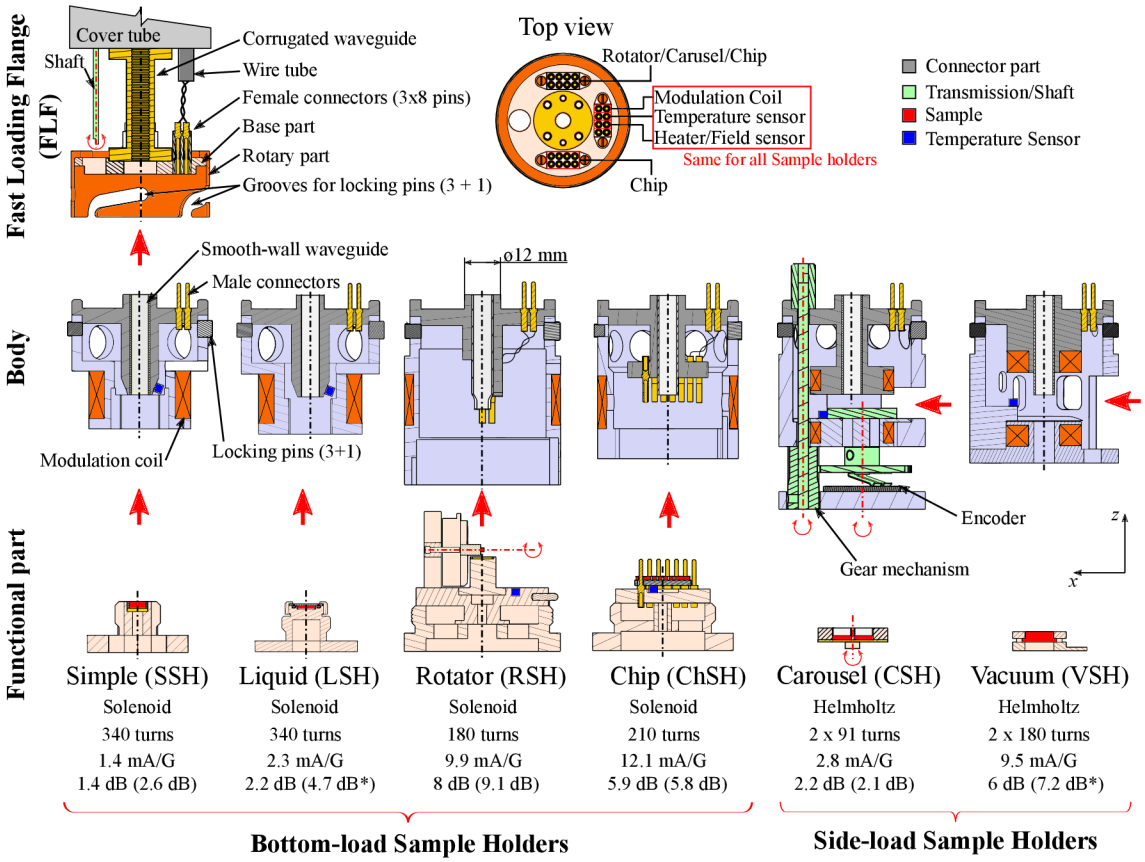

Fig. 4.1: Schematic picture of the sample holders' concept. The SHs can be divided into three parts: FLF attached to the end of the corrugated m.w. waveguide, body of SHs and functional parts, where the samples are located. All functional parts with their respective body are compatible with the FLF. The FLF consists of a set of three 8-connector blocks linked by wires to the probe head connectors, rotary part with grooves for locking pins at bodies, and shaft used in combination with step-motor to exchange sample in the CSH. During loading of bodies into FLF, all electrical contacts and m.w. alignment is made smoothly during the sliding of the locking pins into the grooves by rotating the rotary part of the flange. Furthermore, the bodies can be divided into two groups: *Bottom-load SH* and *Side-load SH* with solenoid and Helmholtz modulation coils, respectively. The *Bottom-load SHs* have a functional part with a sample screwed into the body, whereas the *Side-load SHs* have a sample placed on the platform inserted from the side. The functional parts with location of the SHs are also shown and are described later in text. Additional parameters of the modulation coils, including the number of turns, the current for creating 1 G at 1 kHz modulation, the m.w. attenuation at 430 GHz, and the average of m.w. attenuation of the assembled SHs measured in frequency range (260-500) GHz or (325-500)* GHz are listed.

Inc., USA).

Smooth walled m.w. waveguide out of aluminium has inner diameter 5 mm with the thickness of the wall 0.5 mm. It is pressed into the PEEK connector part of the body and aligned at FLF by a rim of diameter 12 mm to ensure proper m.w. coupling.

Functional parts: All functional parts are designed to enable a visual and manipulation access to the sample, helping with its alignment and visual check outside of the SH body (for example by an optical microscope). The six functional parts for different sample types are described individually with illustrative HF-EPR measurements. Mirrors are made of about 10 nm of gold deposited on 1 μm of aluminum to prevent oxidation on a 500 μm thick silicon wafer.

4.1 Desctription of Sample Holders

The six functional parts for different sample types are described individually with HF-ESR measurements:

Simple Sample Holder (SSH)

has the simplest functional part (Fig. 4.2). It is used for powder samples pressed into pellets of diameter 5 mm and thickness of (1-3) mm, or other solid materials (wafers or crystals) placed directly on the mirror with maximal dimension of cube with the edge 3.2 mm in order to fit in 5 mm diameter. The SSH functional part is manufactured from PEEK, is equipped with a 5 mm diameter smooth-wall cylindrical waveguide and a mirror at the bottom. This part is screwed into the body during the measurement, where the corresponding waveguides are aligned with a minimal gap. The simple construction results in the holder with the lowest attenuation of the m.w. (double pass) 1.4 dB (2.6 dB) at 430 GHz (average attenuation between 260-500 GHz) (see Fig. 4.1).

Fig. 4.2 shows test EPR measurements for this holder on $Mn_{12}Ac$ presented as a EPR map. $Mn_{12}Ac$ is a coordination compound with the total spin S = 10. The presented data shows that the sample holder is capable of measuring in both the frequency and field domains.

Liquid Sample Holder (LSH)

is designed to study liquids or air sensitive samples, has a similar design to SSH with a few adaptations to the functional part, such as a viton o-ring and a sapphire

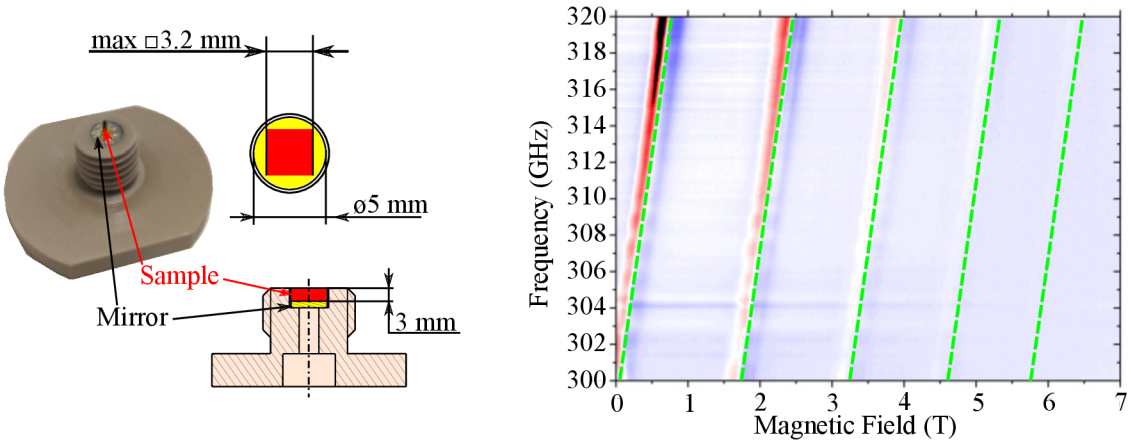

Fig. 4.2: Left) Photograph and drawings of the SSH functional part. A sample in the form of a crystal or a press powder pellet is fixed on the mirror by an EPR silent vacuum grease inside a 5 mm diameter waveguide. The maximal size of crystal that can be loaded into the SSH, is a cube of edge 3.2 mm. Right) The measurement are showing EPR map 1200x800 resolution of $Mn_{12}Ac$ crystal together with simulation (green lines).

window with a nut placed on top. A nut (PEEK) seals the sample cell upon screwing into a thread on the top of the functional part (Fig. 4.2). The hermetically sealed cell can hold volatile liquids in a vacuum environment for weeks. Since our system also operates in the FDMR regime, the studied solution is placed directly on the mirror surface (located at the bottom of the sample cell), where the magnetic field component B_1 of the m.w. has its maximum amplitude [68]. The functional part can be manufactured with a groove of different depths for solvents with higher or smaller dielectric losses to get the best possible SH performance [69]. The attenuation of the m.w. is 2.2 dB (4.7 dB) at 430 GHz (average attenuation between 325-500 GHz) in an empty LSH. Apart from the 1-mm thick sapphire window in the m.w. pathway, LSH and SSH have a similar design, and therefore similar attenuation figures.

The data presented in Fig. 4.2 display the high-frequency measurements of 1 mM TEMPOL dissolved in acetone. We found out experimentally that a 4-mm deep groove with 40 μL of solution provides good EPR signal.

Rotator Sample Holder (RSH)

is designed to rotate samples such as single crystals or thin films in the magnetic field during the HF-EPR measurements. The information extracted from those measurements can provide detailed information about anisotropy of magnetic interactions in paramagnetic materials or solid-state phenomena as cyclotron resonances

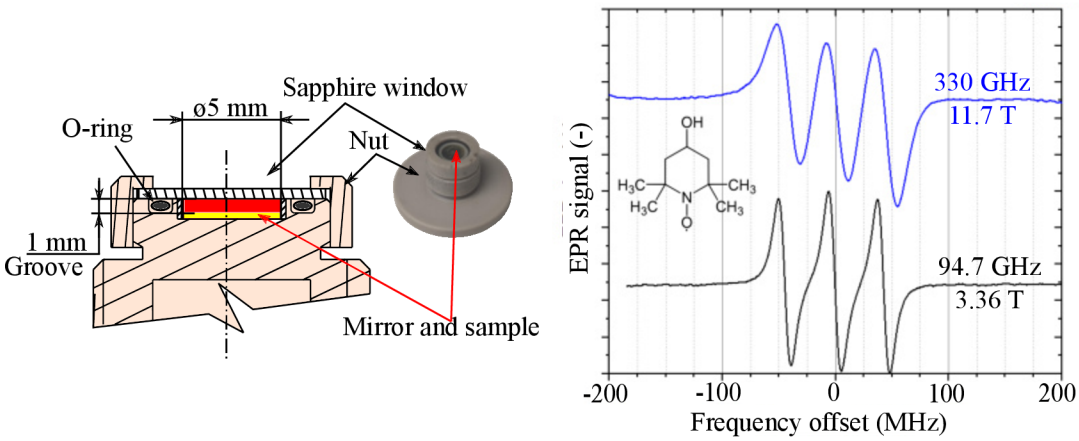

Fig. 4.3: Photograph and drawings of the liquid SH's functional part. The liquid sample is hermetically sealed in a cell with the o-ring and 1 mm thick sapphire window. The functional part can be manufactured with a different groove deepness according to the solvent needed for the measurements. B-Bottom) Frequency domain magnetic resonance (FDMR) measurement of 1 mM of TEMPOL in acetone at 330 GHz and 94.7 GHz at 300 K. The sweep time was 500 ms, with a field modulation of 6 G at 41 kHz. The final spectra is the average of 64 measurements acquired by lock-in amplifier.

in conducting materials [70–74].

The functional part consists of several cylindrical parts with holes providing a steady flow of Helium around the sample for a faster cooling down time. The top rotary base with the leading pin has one degree of freedom and can rotate 360 degrees. Three leading pins in the functional part and the guiding grooves in the body guarantee the correct alignment of the electrical contacts while the rotary base of the functional part allows transferring the rotary motion of the screw to linear motion. The unique position of the three leading pins ensures only one possible loading position (Fig. 4.4,). The RSH's functional part provides 11 contacts, five of them are used for the piezo-rotator (2) and built-in encoder (3), the remaining contacts are for T-sensor and an eventual heater or field sensor. A crystal sample is located on the sapphire rod (Crytur a.s., CZE), which is connected directly to a piezo-rotator (ANRv51/RES/LT, Attocube systems AG, DE). It can work at temperatures below 4 K, in UHV and high magnetic fields. Moreover, it has a built-in encoder allowing measurements with very fine resolution of 0.006 ° (Fig. 4.4 C). The direct connection of the sapphire rods minimizes errors caused by the rotation.

The mirror is placed 2 mm under the axis of the sapphire rod. So far, we have designed and manufactured two sapphire rods. One with a semicylindrical shape, the

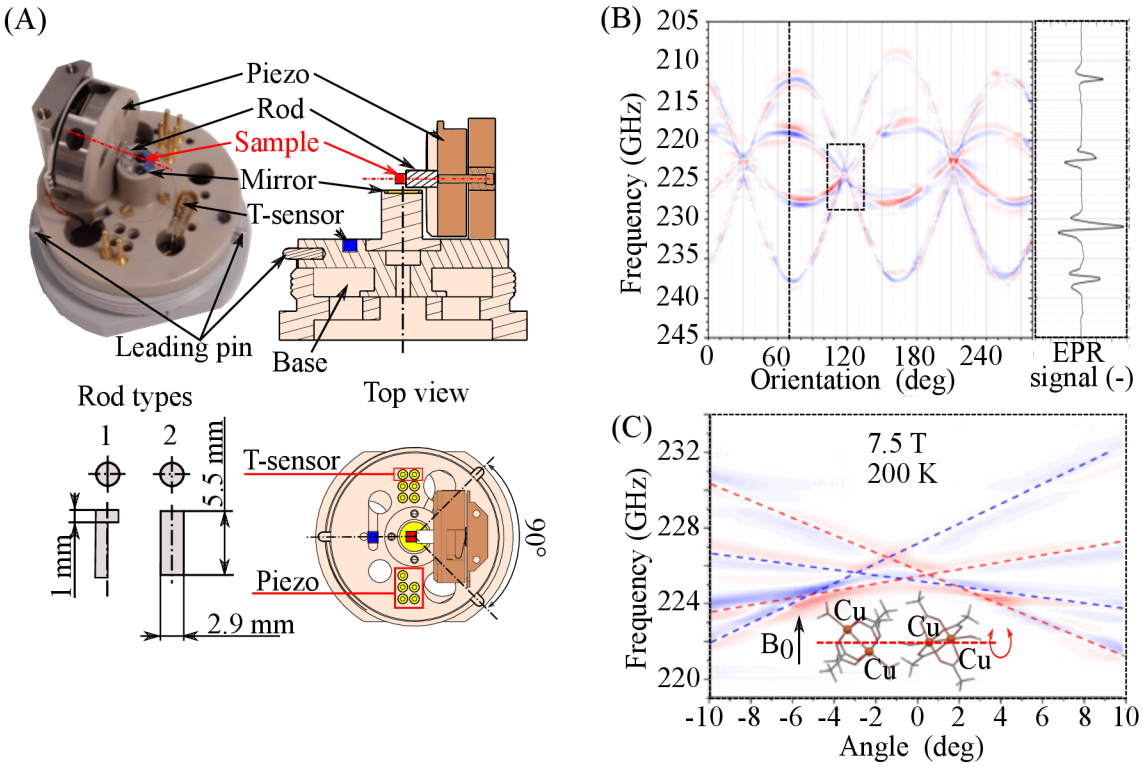

Fig. 4.4: A) Picture and drawings of the RSH functional part, rod types and top view. A sample is glued on the sapphire shaft by an EPR silent vacuum grease, eicosan or epoxy. Depending on the experiment, two types of rods are available. The first, with a *semi-cylindrical* shape, is mainly used for studying thin-layered materials (the maximal thickness of the layer is 1.2 mm). The second, with *cylindrical* shape, is used for studying crystals with a maximal size of a cube with 2.5 mm edge. The necessary electrical connection for piezo and T-sensor are connected automatically during the screwing of the functional part into the SH's body. The leading pins with unique orientation prevent the unwanted exchange of contacts. B) The rotation map of Copper acetate from 0 to 280 ° at a magnetic field of 7.5 T. The detail in the right displays a spectrum of one frequency sweep at 70 °. The acquisition time of each FDMR spectrum is 16 s, and the map was measured in 103 minutes. C) A detailed map at the crossing of the EPR lines with an angular step of 0.1 °.

second rod has a cylindrical shape. To increase m.w. propagation the waveguide is prolonged down to the mirror with a cutout only for the sapphire rods (see Fig. 4.1). However, due to its complex structure, it has the largest return losses out of all SH, at 430 GHz (average attenuation between 260-500 GHz) the return losses are of 8 dB (9.1 dB) with the semicylindrical sapphire rod.

The Fig. 4.4 in the middle and bottom displays FDMR rotation maps for a single crystal of copper acetate monohydrate [$Cu(CH_3COO)_2 \cdot H_2O$]. The four EPR signals observed at a single field/frequency correspond to the m.w. absorption by two rotated molecules in the lattice of this compound. The 0-280° map was obtained by performing automated FDMR measurements and simultaneously rotating the crystal by a 1° step, whereas the detailed map in the range -10°-10° has a 0.1° step. This methodology with FDMR decreases measurement time from days to hours, comparing to a field-domain measurement, and still, the spectrum at a single orientation can be extracted from the map.

Chip Sample Holder (ChSH)

allows characterization of electrical/electronic devices under m.w. irradiation or to perform magneto-transport measurements [75]. The functional part contains 20 connectors, 16 of them host a chip expander, while the other four connect the T-sensor and the heater. The chip expander is a small printed circuit board (PCB) with 16 gold deposited holes and contacts, prepared for wire-bonding of samples [75].

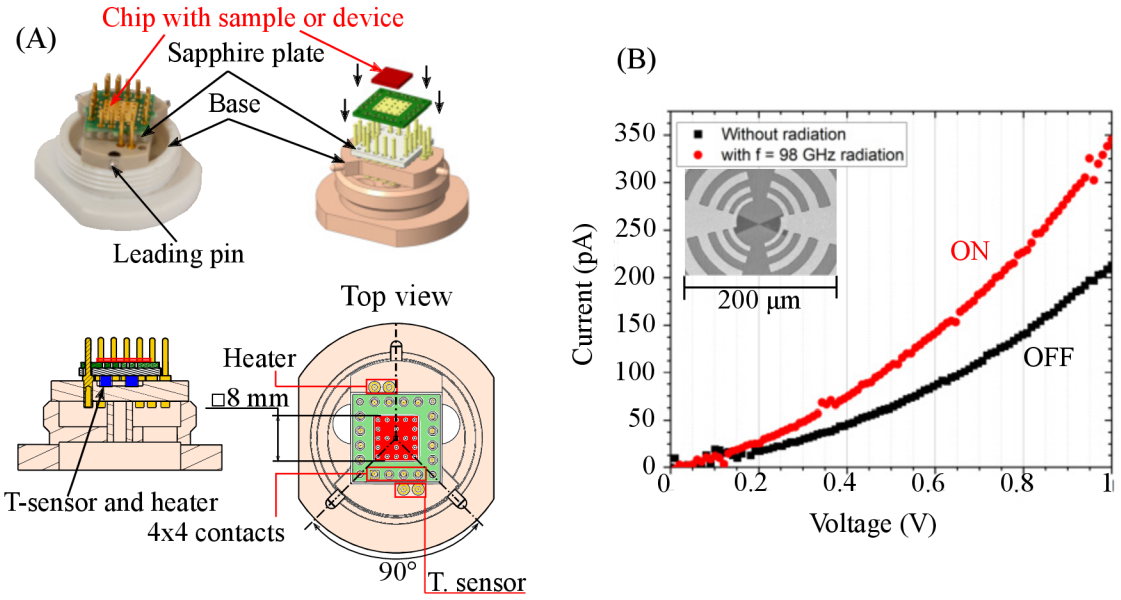

Fig. 4.5: A) Picture and drawings of the ChSH functional part. The T-sensor and the heater are under the sapphire plate, which works as a heat buffer. The sample is glued on the chip that is inserted into the male connectors of the functional part. The inter-space between the contacts is slightly bigger than the inter-space between the holes in chip, ensuring good electrical contact at any temperature. B) Measurements of a graphene bolometer's I/V curves with (ON) and without (OFF) m.w. irradiation at 15 K. The design of the bolometer is in the inset of the plot.

The maximal sample size which can be wire bonded is 8 mm x 8 mm. A small mismatch fit between the electrical connectors and the chip expander's holes guarantees tension for reliable connection. Any device prepared and wire-bonded to the chip expander can be easily loaded with the minimal user interaction (see Fig. 4.5). A sapphire heat sink is placed under the chip expander in order to dissipate the heat effectively to the sample [76]. The T-sensor and the heater are glued to the bottom side of the sapphire plate, which allows precise temperature control of the sample with an stability in the order of 10 mK. Furthermore, the effective Helium cooling is provided by holes in the functional part. Similarly to RSH, three leading pins in the functional part and the guiding grooves in the body guarantee the correct alignment of the electrical contacts, while the rotary base of the functional part allows transferring the rotary motion of the screw to linear motion. After screwing the functional part there is a gap between the sample and the waveguide to avoid touching wire bonds on the sample, resulting in a backward reflected EPR measurements with 5.9 dB (5.8 dB) loss at 430 GHz (average attenuation between 260-500 GHz).

The Fig. 4.5 shows an example of I/V characteristics of a graphene bolometer [77]. We tested the bolometer response to microwave radiation at 98 GHz (red line). The I/V response with (ON) and without (OFF) m.w. irradiation was measured at zero external magnetic field applied. The shift in curves is caused by m.w. irradiation and changes in the bolometer resistance. This represents the characteristic behavior of the bolometer [77].

Carousel Sample Holder (CSH)

was designed to load up to six samples in individual cells simultaneously inside a side loaded rotary platform in the functional part (see Fig. 4.6). The process of changing sample directly inside the magnet significantly reduce spectrometer usage time. With the carousel implementation, the user can switch between six samples directly in the cryostat without unloading the probe, thus saving overall up to 30 h. Moreover, one of the six cells can be used for the system optimization/calibration using a reference sample. Additionally, CSH is the best possible solution for future quantitative high field EPR applications, because the samples is switched directly inside the SH without changing the m.w. coupling. Each sample cell is 5 mm in diameter and 4 mm deep. For better m.w. propagation, the cells' walls are made from an aluminium smooth-wall waveguide as in the corresponding body.

The precise position of the sample cells with respect to the body's waveguide is achieved by a piezo step motor (PiezoMotor Uppsala AB, SE) located outside of the cryostat. It is connected through a shaft to a gears mechanism in the body (Fig. 4.1) and with the rotating platform (functional part). With a 0.01 ° motor step

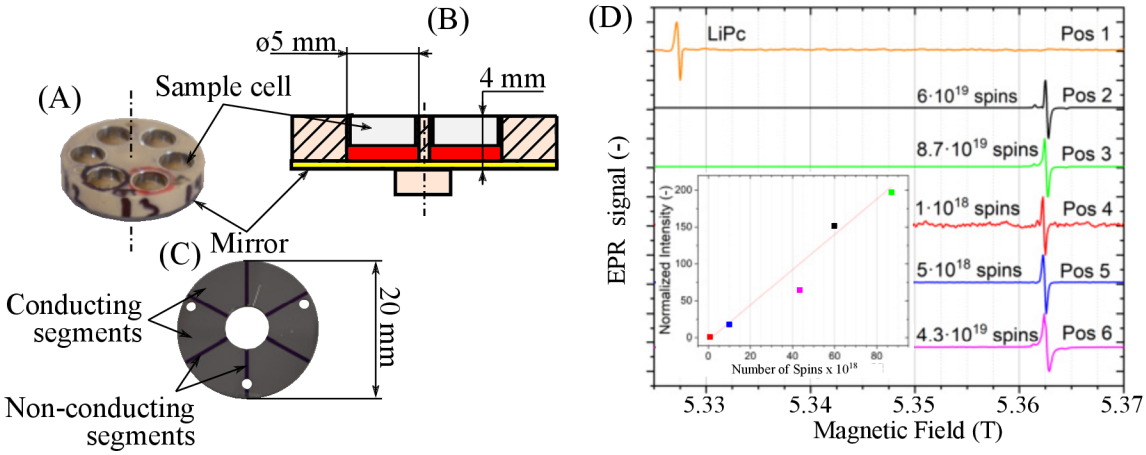

Fig. 4.6: A) Picture and B) drawings of the 6-cell rotary platform of the CSH. Samples are glued on the rotary C) platform's mirror by an EPR-silent vacuum grease. The mirror is divided into conducting and non-conducting segments, reducing the eddy-currents created by the modulation coil. D) Cw-EPR measurements using the different cells at room temperature loaded at once (five BDPA samples with different concentration and one reference LiPc sample). The magnetic field sweep was 0.5 mT/s with field modulation of 10.1 kHz and amplitude 30 G. The measurements are normalized to the intensity of the weakest spectrum (red). The inset shows the plot of the normalized intensities for each sample against their number of spins. Changing among different samples takes a few seconds with the SH placed inside the magnet VTI.

and a gear mechanism (gears ratio 1/5) made from brass, we have the theoretical step precision of 0.002 °. To ensure proper m.w. coupling between the body and functional part, the positioning system is composed of a potentiometer/encoder ring (a graphite/silver thick film on the ceramic substrate, made by SEANT Technology s.r.o., CZE) glued to the bottom of the SH's body and a slider made of phosphor-bronze mounted directly to a bigger gear whose axis is parallel to the encoder axis and the sample functional part axis (Fig. 4.1). The feedback control of the SH is performed automatically via a script included in the home-built LabVIEW software of the FRaSCAN spectrometer. With this system, we can change the sample cell within our temperature working range with the precision of 0.05 ° and ensure good m.w. coupling. The m.w. attenuation in the CSH is 2.2 dB (2.1 dB) at 430 GHz (average attenuation between 260-500 GHz).

Preliminary results of our quantitative EPR measurements are shown in Fig. 4.6. The CSH was loaded by five differently concentrated α,γ-Bisdiphenylene-β-phenylallyl (BDPA) samples and one LiPc reference sample. The intensity of BDPA signal from

each sample follows its concentration (see insert in Fig. 4.6).

Vacuum Sample Holder (VSH)

in combination with a mobile UHV suitcase allows to study air-sensitive structures prepared in a UHV chamber. It is based on an Omicron plate (Scienta Omicron GmbH, DE) for transporting air-sensitive samples which are often manufactured and studied in UHV systems (Fig. 4.7).

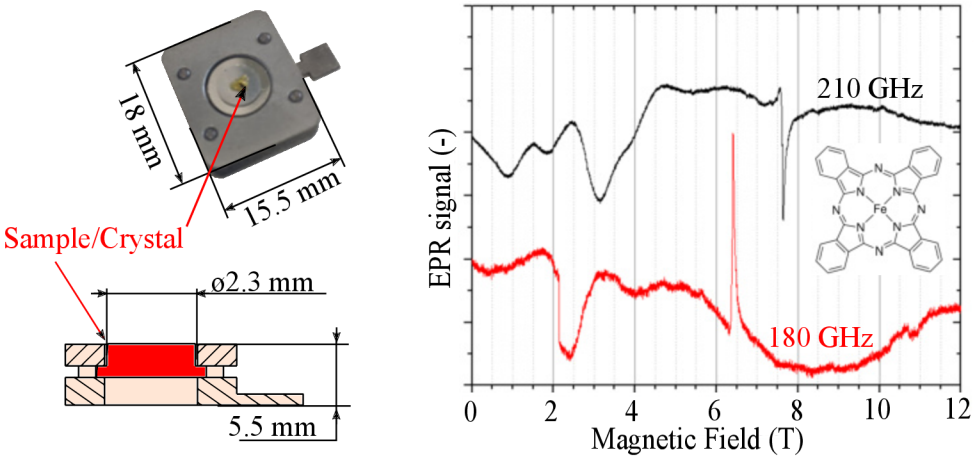

Fig. 4.7: Left) Picture and drawings of the VSH's functional part. The different crystals made of aluminum, gold, silver, or copper can be fixed between two Omicron plates, and the studied structure is then deposited on the top of it. Right) The cw-EPR measurements of Fe-Pt pressed-powder pellet placed on the functional part.

A sample in the form of a deposited layer on a single crystal of Copper, Gold, Iridium etc. (Structure Probe Inc., USA) or on a wafer is fixed to the Omicron plate and side loaded into the VSH. A crystal or a wafer serves as the mirror for EPR measurements. The m.w. attenuation of the holder is 6 dB (7.2 dB) at 430 GHz (average attenuation between 325-500 GHz). However, the size of the crystal and the metallic plate decreases efficiency of modulation coil (Fig. 4.1). Thanks to the VSH, HF-EPR measurements are possible in addition to the XPS (X-ray photoelectron spectroscopy), STM (Scanning Tunneling Microscopy), LEED (Low-Energy Electron Diffraction), and other techniques often used in nano-fabrication clusters [78–80].

The proof of concept EPR measurements were done with pressed-pellet of Iron(II) phthalocyanine (FePc) placed on the Omicron plate (Fig 4.7), one of the candidate for future deposition in UHV.

5 Rapid Scan Measurements

This chapter presents the Rapid Scan measurements performed in the FRaSCAN EPR.

Sensitivity The sensitivity of the spectrometer was determined from the dependence of the SNR on sample spin concentration. The absolute sensitivity was measured for SSH. Sample, DPPH in polystyrene, was made with concentration of 10^{15} spins (number of spin in the whole sample) and measured at 100 GHz. The detection bandwidth (1 ms) and modulation 15 G was used. The measurement results in SNR of 320, then the absolute sensitivity for SSH is:

$$N_{SSH-minimal} = \frac{10^{15}\,\text{spins}}{320 \cdot \sqrt{1\,\text{Hz}} \cdot 15\,\text{G}} = 2 \cdot 10^{13}\text{spins}/(\text{G} \cdot \sqrt{\text{Hz}}). \tag{5.1}$$

Compared to the spectrometer described in reference [35] with sensitivity $5 \cdot 10^{10}$ spins, our sensitivity is worse. The low sensitivity is caused by performing the measurements at 150 GHz and 100 GHz ranges, where the QO is not well-optimized. Moreover, the result shown in [35] were obtained at 320 GHz and 60 K, using bolometer as the detector, which have generally higher sensitivity.

Rapid scan measurement at high frequencies This section is the summary of the article [81]. For the case when the resonance line contains only homogeneous broadening, the EPR spectrum can be simulated, and T_2 relaxation time can be numerically extracted [81]. However, the rapid scan spectrum at high frequency also contains non-homogeneous broadening. The broadening is caused by (hyper)fine structure, g-factor anisotropy, g-strains, and nonuniform magnetic field distribution over the sample. Fig. 5.1 shows the fit of the rapid scan signal with homogeneous and non-homogeneous broadening at 430 GHz. The non-homogeneous broadening precludes the equations in subsection *Rapid Scan Theory* to simulate rapid scan with an additional parameter. Moreover, the experiment needs to be changed too. Due to broader lines, the necessity of faster sweep rates as the condition becomes:

$$\left|\frac{d\omega}{dt}\right| \geq \Delta\omega^2, \tag{5.2}$$

where $\Delta\omega$ is the half-width at half maximum of the slow scan EPR spectrum characterized by relaxation time:

$$T_2^* = \frac{1}{\Delta\omega} < T_2. \tag{5.3}$$

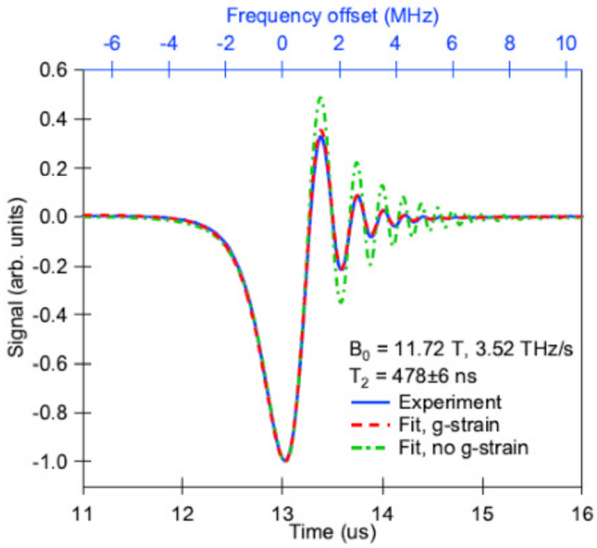

Fig. 5.1: An example of rapid scan ESR acquired on a single microcrystal of LiPc (blue) and its fit with homogeneous (green) and in-homogeneous (red) broadening models. Incident microwave power is 1mW, 10^4 averages, total acquisition time is 5 s. Published in [81].

The sweeps rates are not such a problem in the modern spectrometer, where rapid scan on any ESR line with $\Delta\omega$ up to 100 MHz can be recorded [28]. However, to be able to simulate non-homogeneous broadening, the Bloch equation has to be modified by an additional relaxation mechanism. Such a modification is rather complicated as there typically several non-homogeneous broadening sources are involved. Regardless of the origin of non-homogeneous broadening, the resulted slow scan ESR spectrum is a sum of contributions from individual spin packets. The individual rapid scan responses from the overall spectrum can be written:

$$r(t) = (\sum_i s_i * d)(t) = \sum (s_i * d)(t) = \sum r_i(t). \tag{5.4}$$

Then, the rapid scan spectrum of a complex system can be obtained as a weighted of these sum of the solutions of the Bloch equations. The demonstration of this theory was done on LiPc crystal needle (see Fig. 5.1). The benefit of LiPc is an extremely narrow signal width of 50 KHz at X-band [82]. The linewidth became broader with higher frequencies. That can indicate the shorter spin-spin relaxation time T_2. The origin of the non-homogeneous broadening in LiPc is probably unresolved hyperfine splitting from Li and N nuclei and g-factor strain. Fig. 5.1 shows that without the g-strain (green), the oscillation is more dominant than simulation with g-strain (red), which matches well with the experiment data. The simulation

with the g-strain was done by calculating 30 rapid scan spectra with the normal distribution of g-factor, then they were summed up with the corresponding weights.

Rapid Scan with the Rotator Sample Holder This section presents a study of the spin relaxation of crystals during their rotation in a magnetic field using the RSH. The test sample, LiPc crystal, was glued by epoxy to the rotator rod, and then rapid scan measurements were performed with different orientations (see Fig. 5.2). The spectra were obtained at room temperature and B_0 of 5.5 T, corresponding to the m.w. frequency in the 150 GHz range. Even without quantitative analysis, it is seen that the oscillations' amplitude is smaller for the crystal orientation perpendicular to the magnetic field, meaning the shorter spin relaxation time. The spectra simulation with the modified Bloch equations resulted in $T_2 = 305$ and 370 ns for the perpendicular and 45 ° orientations.

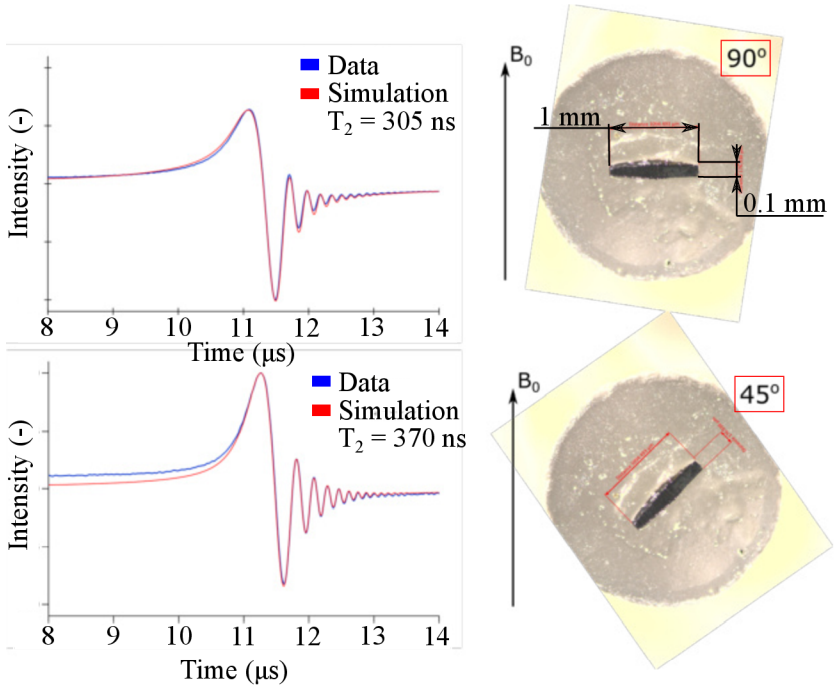

Fig. 5.2: Rapid scan measurement on LiPC with the different crystal direction to magnetic field B_0. Sample was glued to the rod of RSH by epoxy. Parameters of the measurement: $B_0 = 5.452$ T, T = 293 K, frequency sweep 152.56 - 152.63 GHz, number of averages 2 000 000.

From the measurements performed with pulse X-band EPR [83], it is known that LiPc has the slowest spin relaxation when the crystal is oriented perpendicularly to the external field B_0.

Rapid scan on radicals with Liquid Sample holder In this section, the combination of Rapid scan with the LSH is presented. The measurement in Fig. 5.3 demonstrates the proof of concept and the possibility of using our spectrometer to study the relaxation time of radicals in liquid solutions.

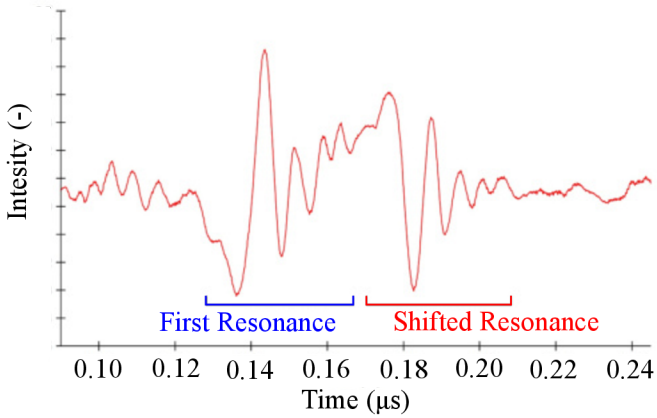

Fig. 5.3: Rapid scan measurement of 2mM BDPA dissolved in toluene. The not-degassed sample ($\approx$ 50 nl) was sealed in LSH. The parameters of the measurements: frequency generated by AWG at 390 GHz in chirp pulses of 1.8 GHz (V Shape), sweep rate 0.5 μs, T=293 K, $B_0 \approx 14$ T, number of averages = 2 000 000.

BDPA dissolved in toluene at 2 mM concentration was measured at 390 GHz. The sample was not degassed, making the signal broader and less intense due to the presence of oxygen [84]. Two resonance signals result from shifting the main signal (see Fig. 5.3 blue) via DC in the modulation coil. Higher current, which would shift the second resonance out of the measurement spectra, was not used due to the limit of the used current source (2.5 A). Our synthesizers could not sweep sufficiently fast over the signal area in these particular measurements. Therefore, AWG replaced them to generate a broader sweep (chirp pulses of 1.8 GHz (V Shape) with a sweep rate of 0.5 μs.), which was necessary to see rapid scan oscillations. Moreover, the detector mixers were replaced by zero bias detectors due to unstable dual-channel AWG output, resulting in the wrong synchronization of LO and RF lines. The final spectrum is the result of 2 000 000 averages. Despite that, the background of the spectrum is significant, which made it impossible to simulate the rapid scan signal. This measurement is proof of the applicability of our spectrometer for the study relaxation times of radicals but further work will be needed to improve the method.

Conclusion

This work focused on the development of an EPR spectrometer with the main goal of measuring relaxation times via Rapid Scan, called FRaSCAN EPR. The main properties of the FRaSCAN Spectrometer are frequency range $80 - 1100$GHz, magnetic field range 0 ± 16 Tesla, Sample temperature from $2 - 400$ K, and possible to run continuous wave EPR experiments in field domain and frequency domain (even simultaneously), and rapid scan EPR. This thesis is split into two main parts, the theoretical and practical ones.

The spectrometer consists of three standalone parts: magnet frame, EPR table, and EPR probe. The magnet frame holds the superconducting cryogen-free magnet in the lab pit. Therefore, loading the sample into the magnet is in an user-friendly height. Furthermore, the magnet frame contains the automated docking desk with all electronics, computer ports, and the servo-driven movement system for coupling different tables with the superconducting magnet. The switching of tables was demonstrated with FIR and EPR tables. One important part of the magnet frame is the designed airlock system, which allows loading the EPR probe into the magnet VTI without air contamination. The airlock was designed with a side valve and window, which allows the transfer of sensitive samples into the probe inside the airlock via a designed UHV transfer case. The EPR table has a frame with a retractable wheel which allows it to be undocked from the magnet frame. The EPR table contains all electronics and m.w. components, which are needed for the EPR experiment. It contains m.w. sources and detectors, quasi optics solution to couple the m.w. with EPR probe, electronics needed for EPR experiments (lock-in, digitizer, source-meter. power sources), and four servo-driven movement systems for automatic m.w. coupling between the EPR table and EPR Probe. Proof-of-concept test shows that automatic procedure significantly reduces the time needed to couple the m.w. beam between the table and probe. The last part of the spectrometer is the EPR probe. The EPR probe is the long corrugated waveguide shielded by a stainless tube with an opened bottom end and with window at the top. The stainless steel tube serves for differential pumping during the loading of the EPR probe into the magnet through the airlock. At the bottom of the EPR probe is the FLF, which reduces the sample holder preparation and loading to a minimum time. Thanks to FLF, wiring, and m.w. coupling of the sample holder is reduced to the minimum. The part of the design was also the study of m.w. attenuation by VNA and Tk power meter, study the cooling dependence of the EPR probe, and testing and troubleshooting of all mechanical parts.

In total, six different sample holders were designed and troubleshot. All sample holders are shown together with the measurement as the proof-of-functionality. SSH

for measuring press powder pellets or crystals with Mn_{12} EPR map, RSH for oriented crystal measurement with rotary map measurements of copper acetate, ChSH for testing devices under m.w. with the test of the bolometer, Liquide SH for measuring liquid samples with measurement TEMPOL dissolved in acetone, CSH for measuring up to six press powder pallets with the example of quantitative EPR measurements done with five differently concentrated BDPA samples, and VSH for measure air-sensitive samples prepared in UHV cluster with measurement of press powder pallet. Moreover, m.w. VNA studied attenuation in sample holders to improve overall performance. VNA measurements were used for the inner diameter of the waveguide optimization and to know which frequencies to avoid during the EPR experiments for each sample holder.

The end of this thesis is focused on rapid scan measurements. At the beginning is shown how to calculate the sensitivity. Even the sensitivity ($5 \cdot 10^{14}\,\mathrm{spins}/(\mathrm{G} \cdot \sqrt{\mathrm{Hz}})$) results to below others HF-EPR spectrometer ($5 \cdot 10^{10}\,\mathrm{spins}/(\mathrm{G} \cdot \sqrt{\mathrm{Hz}})$) [35], the spectrometer is under constant development. As the specter's troubleshooting continues, I believe that this number will decrease to the point that spectrometer sensitivity will get to the state-of-the-art point. Even while I was finishing this thesis, the crucial problem in orientation XP mixer, which attenuates signal by 3 dB, was found. Nevertheless, I would like to mention a few suggestions that would be worth investigating in the future to improve spectrometer sensitivity:

- First of all, the ground of the detectors. The noise of different frequencies was present from time to time during the measurements. I would recommend avoiding any ground loops which would be found. Moreover, all the grounds should be connected to one line separated from the power grid.
- Secondly, I would recommend a more deep analysis of XP isolation and leakage from CO into XP when the m.w. propagate into the EPR probe. We recently found out that there is quite a big leakage of LO into the XP detector. The origin is unsure yet. It is mainly visible when the high power output of m.w. source is used. If the origin is in the probe, one solution might be to implement a roof mirror that can rotate under the sample to increase XP isolation.
- Thirdly, I recommend checking the modulation coil wiring connection as some modulation frequencies create random signal steps in EPR spectra.

The last chapter shows a series of rapid scan EPR done with LiPC, ending with proof-of-concept a rapid scan on the radicals, not degassed sample of DPPH dissolved in toluene, which was the main task of my Ph.D.

Perspectives: Despite the fast development of magnetic resonance field, I hope that this thesis will remain up-to-date and provide useful information to anyone who will read it. A HF-EPR spectrometer is high complexity and not easy to build

and operate. In my work, I pointed out that any spectrometer using a sample holder without a resonator (non-resonant sample holder) has a wide range of applications, which can be reached by designing appropriate sample holders. There are plenty of problems that still need to be solved in the development of rapid scan EPR. How to make stable broad sweep, background treatment for broad signals, measurement of T_1 time and more. Still, even little progress of EPR spectroscopy can bring new information in many scientific disciplines.

We prove that our spectrometer can perform rapid scan on the samples with a relatively narrow signal like DPPH or LiPC. Next progress in frequency domain rapid scan will open the door of the new broad use of EPR. Thanks to broader operating range (tens of GHz) and the absence of a dead time, rapid scan can theoretically measure extremely short T_2 (ns) relaxation times at any frequency within the spectrometer's frequency range. Therefore, as the sensitivity of detectors and spectrometer goes higher together with more powerful and faster m.w. sources, we can expect measuring T_2 and T_1 time on samples with broad line width such as transition metals complexes, SMM/SIM quantum bits, and others. Moreover, our successful experiment on DPPH will open the door for DNP radical study in the near future. The development of rapid scan on radicals dissolved in liquid will continue in our EXPRO GAČR project (Implementation of Frequency Rapid Scan Electron Spin Resonance Spectroscopy into Nuclear Magnetic Resonance Systems), which recently received financial support. The successful study of such radicals in high magnetic fields is necessary in understanding and optimizing the nuclear polarization efficiency and developing spin polarization agents. Thus, significantly improve the NMR spectroscopy.

Author publications and other outputs:

- **PUBLICATION**

2022 Sample Holders for Sub-THz Electron Spin Resonance Spectroscopy, IEEE Transactions on Instrumentation and Measurement, ***A. Sojka****, et al. (Submitted)*

2021 Rapid scan ESR: a versatile tool for the spin relaxation studies at (sub)THz frequencies, Applied Physics Letters, *O. Laguta,* ***A. Sojka****, et al. (Accepted)*

2021 Simulation of nitrogen nuclear spin magnetization of liquid solved nitroxides, Phys Chem Chem Phys, *Andriy Marko,* ***A. Sojka****, et al.*

2020 High-frequency EPR: current state and perspectives, RSC Electron Paramagnetic Resonance: Volume 27, 214 – 252. ***A. Sojka,*** *et al.*

2020 Deposition of Tetracoordinate Co(II) Complex with Chalcone Ligands on Graphene, Molecules, 25, 5021. *J. Hrubý, Š. Vavrečková, L. Masaryk****, A. Sojka,*** *et al.*

- **CONFERENCES/SUMMER SCHOOLS**

09/2021 PhD Retreat 2021 (online), Czech Republic

04/2021 (Poster) RSC ESR 2021 (online), Scotland

11/2019 (Poster) 8th European Federation of EPR School, Czech Republic, **Member of Organizers**

09/2019 (Poster) XIth EFEPR Conference, Bratislava, Slovakia

07/2019 (Poster) 60st Rocky Mountain Conference on Magnetic Resonance, Denver (USA)

06/2019 (Talk) 2nd conference of the Magneto-Optical and THz Spec. Research Group, Poland

10/2018 (Poster) PETER Summer School, Brno, Czech Republic

09/2018 (Talk) V International School for Young Scientists, Russia

07/2018 (Poster) ICN+T, Brno, Czech Republic. **Member of organizers**

04/2018 (Poster) CEITEC PhD & Postdoc Retreat, Telč, Czech Republic, **Winner of Poster price**

07/2017 16th IUVSTA International Summer School on Phys. at Nanoscale, Czech Republic

03/2016 (Poster) sIMMposium Symposium of the Institute Molecules and Materials, Netherlands

02/2015 (Poster) Brno University of Technology students poster session, Brno, Czech Republic

- **INTERNSHIPS**

2019 CEITEC Mobility, Santa Barbara University, USA, group of prof. Mark Sherwin.

2017 COST+, University of Stuttgart, Germany, group of Prof. Dr. Joris van Slageren.

2016 Erasmus+ program, Radboud University, Netherlands, Group of Prof. Alex Khajetoorians.

- **EDUCATION**

2015 – 2017 Master's study at Brno University of Technology, Institute of Physical Engineering and Nanotechnology (Czech Republic) under the supervision of Ing. Michal Pavera Ph.D.
Master's Thesis: *Low-temperature scanning tunneling microscopy*

2012 – 2015 Bachelor's study at Brno University of Technology, Institute of Physical Engineering and Nanotechnology (Czech Republic) under the supervision of Ing. Michal Pavera Ph.D.
Bachelor's Thesis: *Assembling and testing of the STM microscope*

2008 – 2012 Grammar school, Gymnázium Rožnov pod Radhoštem, Czech Republic

- **CURRENT POSITION**

2017 – Present Ph.D.'s study at the Central European Institute of Technology (CEITEC), Brno (Czech Republic) under the supervision of Dr. Ing. Petr Neugebauer.
Topic: *Development of a Terahertz Magnetic Resonance Spectrometer for Electron Spin Dynamics Investigations*

- **PREVIOUS POSITIONS**

2020 R&D Designer, company Activair s.r.o., Brno, Czech Republic. *Development of a high-vacuum chamber for the study of welds.*

2016 – 2017 R&D System engineer, company FEI Thermo Fisher Scientific CZ s.r.o., Brno, Czech Republic. *Development of high-end scanning electron microscopes.*

2015	Lab worker, Institute of Physical Engineering and Nanotechnology, Brno, Czech Republic. *Development of the STM cooling system.*
2014 – 2015	Engineer, Aura engineering Hranice spol. s.r.o., Hranice Czech Republic, D*esing of single-purpose machines*
2008 – 2013	Electrician, Company Sojka, Hluzov, Czech Republic.
Others:	Summer Camp supervisor, *Group leader and game creator for kids 6 – 15 years*

- **SUPERVISION STUDENTS (3 bachelors, 1 high school)**

Tomáš Fargaš	Bachelor, 2021 Topic: *Rapid scans EPR on DNP relevant radicals*
Bc. Adam Lagiň	Bachelor, 2020, Topic: *Design of non-resonant sample holders,*
Bc. Andrej Gabriš	Bachelor, 2020, Topic: *Design of single-crystal sample holder for high-frequency electron paramagnetic resonance,*
Adam Vondráček	High school student, 2019-2020 Topic: *Artificial neural network in EPR* **Best presentation – 2019 and 2020 (CEITEC Student Talent)**

- **CO-SUPERVISION STUDENTS (2 Masters)**

Ing. Tomáš Láznička Master, 2020, Topic: *Design vacuum transfer chamber for High Field – EPR*
Ing. Tomáš Martínek Master, 2018, Topic: *Design of a Non-Resonant General Purpose Sample Holder for Terahertz EPR Spectroscopy*

- **TEACHING ACTIVITIES**

2020 – Present: EPR practical lab courses, 3rd- year students of Institute of Physical Engineering, BUT.
2018 – 2020: Physics lab courses, 1st- year student of Institute of Mechanical engineering, BUT.
2018 – 2020: Physics lab courses, 2st- year student of Institute of Mechanical engineering, BUT.

- **ORGANIZATION OF SCIENTIFIC MEETINGS**

2019	8th European Federation of EPR School
2018	ICN+T , Brno, Czech Republic
Others:	Activities for the popularization of science: *Researchers´ Night (2018 and 2019), VUT Junior (2020), VUT 120 anniversary (2019), excursion for public on CEITEC*

- **MEMBERSHIPS OF SCIENTIFIC SOCIETIES**

2019 – Present: Member of International EPR (ESR) Society

- **AWARDS**

2020	Travel Stipendium for Rocky Mountain Conference on Magnetic Resonance
2019-2020	Adam Vondracek, Best presentation – 2019 and 2020 (young CEITEC scientist)
2018	Winner of Poster price, CEITEC PhD & Postdoc Retreat, Telč, Czech Republic
2017	FEI Thermo Fisher Scientific CZ s.r.o. award for job achievements

- **INVOLVEMENT IN PROJECTS**

2020 - present	CZ-USA Inter-Excellence Topic: *Spectroscopy of single molecular magnets using graphene bolometers*
2019	Internal CEITEC project for creating a new education course, Topic: *Laboratory courses in Electron Paramagnetic Resonance*
2017	COST+, Topic: *Influence of Substrates on Magnetic Properties of Deposited Single-Molecule Magnets*
2017 - present	ERC, Topic: *THz Frequency Rapid Scan – Electron Spin Resonance spectroscopy for spin dynamics investigations of bulk and surface materials*

Bibliography

[1] T. Martinek. Design of a non-resonant general purpose sample holder for terahertz electron paramagnetic resonance spectroscopy, Master's thesis, 2018.

[2] A. Lagiň. Design of non-resonant sample holders, Bachelor's thesis, 2020.

[3] A. Gabriš. Návrh držáku vzorku pro studium orientovaných krystalů pomocí vysokofrekvenční paramagnetické resonance, Bachelor's thesis, 2020.

[4] T. Fargač. Rapid scan epr spectroscopy on dnp relevant radicals, Bachelor's thesis, 2021.

[5] T. Láznička. Design of mobile vacuum chamber for loading samples into high--frequency electron paramagnetic resonance spectrometer, Master's thesis, 2020.

[6] E. K. Zavoisky. Paramagnetic relaxation of liquid solutions for perpendicular fields. *Zhur. Eksperiment. i Theoret. Fiz.*, 15(12):344–350, jul 1944.

[7] L. Kevan and M. K. Bowman. *Modern pulsed and continuous-wave electron spin resonance*. 1990.

[8] A. J. Weil and J. Bolton. In *Electron Paramagnetic Resonance: Elementary Theory and Practical Applications*. 2nd edition, 2006.

[9] O. Duss, M. Yulikov, G. Jeschke, and F. Allain. EPR-aided approach for solution structure determination of large RNAs or protein-RNA complexes. *Nature Communications*, 5, may 2014.

[10] A. Mullen, J. Hall, J. Diegel, I. Hassan, A. Fey, and F. MacMillan. Membrane transporters studied by EPR spectroscopy: Structure determination and elucidation of functional dynamics. *Biochemical Society Transactions*, 44(3):905–915, jun 2016.

[11] P. Consentius, U. Gohlke, B. Loll, C. Alings, U. Heinemann, M. C Wahl, and T. Risse. Combining EPR spectroscopy and X-ray crystallography to elucidate the structure and dynamics of conformationally constrained spin labels in T4 lysozyme single crystals. *Phys. Chem. Chem. Phys.*, 19(31):20723–20734, aug 2017.

[12] M. Carmen Giménez-López, F. Moro, A. La Torre, C. J Gómez-García, P. D Brown, J. Van Slageren, and A. N Khlobystov. Encapsulation of single-molecule magnets in carbon nanotubes. *Nature Communications*, 2, 2011.

[13] A. Kajiwara and K. Matyjaszewski. EPR and kinetic studies of atom transfer radical polymerization of (meth)acrylates. *Polymer Journal*, 31(1):70–75, 1999.

[14] F. Liu, D. S. Krylov, L. Spree, S. M. Avdoshenko, N. A. Samoylova, M. Rosenkranz, A. Kostanyan, T. Greber, A. U.B. Wolter, B. Büchner, and A. A. Popov. Single molecule magnet with an unpaired electron trapped between two lanthanide ions inside a fullerene. *Nature Communications*, 8, jul 2017.

[15] N. Fujita, D. Matsumoto, Y. Sakurai, K. Kawahara, H. Ago, T. Takenobu, and K. Marumoto. Direct observation of electrically induced Pauli paramagnetism in single-layer graphene using ESR spectroscopy. *Scientific Reports*, 6, oct 2016.

[16] K. Sato, S. Nakazawa, S. Nishida, R. D. Rahimi, T. Yoshino, Y. Morita, K. Toyota, D. Shiomi, M. Kitagawa, and T. Takui. Novel Applications of ESR/EPR: Quantum Computing/Quantum Information Processing. 2012.

[17] A. S. Thankamony, J. J. Wittmann, M. Kaushik, and B. Corzilius. Dynamic nuclear polarization for sensitivity enhancement in modern solid-state nmr. *Progress in Nuclear Magnetic Resonance Spectroscopy*, 102-103:120–195, 2017.

[18] Q. Ni, E. Daviso, T. Can, E. Markhasin, S. K. Jawla, T. M. Swager, R. J. Temkin, J. Herzfeld, and R. G. Griffin. High frequency dynamic nuclear polarization. *Accounts of Chemical Research*, 46(9):1933–1941, sep 2013.

[19] M. N. Leuenberger and D. Loss. Quantum computing in molecular magnets. *Nature*, 410(6830):789–793, apr 2001.

[20] S. Realista, A. J. Fitzpatrick, G. Santos, L. P. Ferreira, S. Barroso, L. C. J. Pereira, N. A. G. Bandeira, P. Neugebauer, J. Hrubý, G. G. Morgan, J. van Slageren, M. J. Calhorda, and P. N. Martinho. A mn(iii) single ion magnet with tridentate schiff-base ligands. *Dalton Trans.*, 45:12301–12307, 2016.

[21] I. Nemec, R. Herchel, M. Kern, P. Neugebauer, J. Van Slageren, and Z. Trávníček. Magnetic anisotropy and field-induced slow relaxation of magnetization in tetracoordinate coii compound [co(ch3-im)2cl2]. *Materials*, 10(3), 2017.

[22] Y.-Y. Zhu, T.-T. Yin, S.-D. Jiang, A.-L. Barra, W. Wernsdorfer, P. Neugebauer, R. Marx, M. Dörfel, B.-W. Wang, Z.-Q. Wu, J. van Slageren,

and S. Gao. The solvent effect in an axially symmetric feiii4 single-molecule magnet. *Chem. Commun.*, 50:15090–15093, 2014.

[23] T. K. Prasad, G. Poneti, L. Sorace, M. J. Rodriguez-Douton, A.-L. Barra, P. Neugebauer, L. Costantino, R. Sessoli, and A. Cornia. Magnetic and optical bistability in tetrairon(iii) single molecule magnets functionalized with azobenzene groups. *Dalton Trans.*, 41:8368–8378, 2012.

[24] G. M. Smith, P. A. S. Cruickshank, D. R. Bolton, and D. A. Robertson. High-field pulse epr instrumentation. In *Electron Paramagnetic Resonance: Volume 21*, volume 21, pages 216–233. The Royal Society of Chemistry, 2008.

[25] J. R. Biller, D. G. Mitchell, M. Tseytlin, H. Elajaili, G. A. Rinard, R. W. Quine, S. S. Eaton, and G. R. Eaton. Rapid scan electron paramagnetic resonance opens new avenues for imaging physiologically important parameters in vivo. *Journal of Visualized Experiments*, 2016(115), sep 2016.

[26] S. S. Eaton, Y. Shi, L. Woodcock, L. A. Buchanan, J. McPeak, R. W. Quine, G. A. Rinard, B. Epel, H. J. Halpern, and G. R. Eaton. Rapid-scan EPR imaging. *Journal of Magnetic Resonance*, 280:140–148, jul 2017.

[27] D. G. Mitchell, G. M. Rosen, M. Tseitlin, B. Symmes, S. S. Eaton, and G. R. Eaton. Use of rapid-scan epr to improve detection sensitivity for spin-trapped radicals. *Biophysical journal*, 105(2):338–342, 2013.

[28] O. Laguta, M. Tuček, J. van Slageren, and P. Neugebauer. Multi-frequency rapid-scan HFEPR. *Journal of Magnetic Resonance*, 296:138–142, nov 2018.

[29] A. Marko, A. Sojka, O. Laguta, and P. Neugebauer. Simulation of nitrogen nuclear spin magnetization of liquid solved nitroxides. *Phys. Chem. Chem. Phys.*, 23(32):17310–17322, aug 2021.

[30] P. Neugebauer, J.-G. Krummenacker, V.-P. Denysenkov, Ch. Helmling, C. Luchinat, G. Parigi, and T.-F. Prisner. High-field liquid state NMR hyperpolarization: a combined DNP/NMRD approach. *Phys. Chem. Chem. Phys.*, 16(35):18781–18787, aug 2014.

[31] P. Neugebauer, J. G. Krummenacker, V. P. Denysenkov, G. Parigi, C. Luchinat, and T. F. Prisner. Liquid state dnp of water at 9.2 t: an experimental access to saturation. *Phys. Chem. Chem. Phys.*, 15:6049–6056, 2013.

[32] S.-E. Küçük, P. Neugebauer, T.-F. Prisner, and D. Sezer. Molecular simulations for dynamic nuclear polarization in liquids: a case study of tempol in acetone and dmso. *Phys. Chem. Chem. Phys.*, 17:6618–6628, 2015.

[33] M. Rohrer, O. Brügmann, B. Kinzer, and Thomas F. Prisner. High-field/high-frequency EPR spectrometer operating in pulsed and continuous-wave mode at 180 GHz. *Applied Magnetic Resonance 2001 21:3*, 21(3):257–274, 2001.

[34] D. Gatteschi, R. Sessoli, and J. Villain. *Molecular Nanomagnets*, volume 9780198567530. Oxford University Press, sep 2007.

[35] P. Neugebauer, D. Bloos, R. Marx, P. Lutz, M. Kern, D. Aguilà, J. Vaverka, O. Laguta, C. Dietrich, R. Clérac, and J. Van Slageren. Ultra-broadband EPR spectroscopy in field and frequency domains. *Phys. Chem. Chem. Phys.*, 20(22):15528–15534, 2018.

[36] J. Hrubỳ, S. Vavrečková, L. Masaryk, A. Sojka, G. J. Navarro, M. Bartoš, R. Herchel, J. Moncol, I. Nemec, and P. Neugebauer. Deposition of tetracoordinate co (ii) complex with chalcone ligands on graphene. *Molecules*, 25(21):5021, 2020.

[37] A. Sojka, M. Šedivý, O. Laguta, A. Marko, V. T. Santana, and P. Neugebauer. High-frequency EPR: Current state and perspectives. *Electron Paramagnetic Resonance*, 27:214–252, nov 2021.

[38] I. Park, Ch. Lee, J. Park, S. Kim, and S. Jeong. Performance of the fast-ramping high temperature superconducting magnet system for an active magnetic regenerator. *IEEE Transactions on Applied Superconductivity*, 27(4):1–5, 2017.

[39] A.L. Barra. High- and multi-frequency epr study of mn12: A new technique for studying new objects. *Inorganica Chimica Acta*, 361(12):3564–3569, 2008. Protagonists in Chemistry: Dante Gatteschi (Part I).

[40] P. Neugebauer. Development of Heterodyne High Field / High Frequency Electron Paramagnetic Resonance Spectrometer at 285 GHz. Technical report, Dissertation's Thesis, 2010.

[41] K. Möbius, A. Savitsky, A. Schnegg, M. Plato, and M. Fuchs. High-field epr spectroscopy applied to biological systems: characterization of molecular switches for electron and ion transfer. *Phys. Chem. Chem. Phys.*, 7:19–42, 2005.

[42] R. Maurice, C. de Graaf, and N. Guihéry. Theoretical determination of spin hamiltonians with isotropic and anisotropic magnetic interactions in transition metal and lanthanide complexes. *Phys. Chem. Chem. Phys.*, 15:18784–18804, 2013.

[43] A. Abragam and B. Bleaney. *Electron paramagnetic resonance of transition ions*. Oxford : Clarendon press, Oxford, first edition, 1970.

[44] X. Feng, J. Liu, T. D. Harris, S. Hill, and J. R Long. Slow magnetic relaxation induced by a large transverse zero-field splitting in a mniireiv (cn) 2 single-chain magnet. *Journal of the American Chemical Society*, 134(17):7521–7529, 2012.

[45] J. M. Frost, K. L.M. Harriman, and M. Murugesu. The rise of 3-d single-ion magnets in molecular magnetism: Towards materials from molecules? , apr 2016.

[46] A. Lund, E. Sagstuen, A. Sanderud, and J. Maruani. Relaxation-Time Determination from Continuous-Microwave Saturation of EPR Spectra. *Radiation Research*, 172(6):753 – 760, 2009.

[47] C. Griesinger, M. Bennati, H. M. Vieth, C. Luchinat, G. Parigi, P. Höfer, F. Engelke, S. J. Glaser, V. Denysenkov, and T. F. Prisner. Dynamic nuclear polarization at high magnetic fields in liquids, 2012.

[48] E. Moreno Pineda, N. F. Chilton, R. Marx, M. Dörfel, D. O. Sells, P. Neugebauer, S. D. Jiang, D. Collison, J. Van Slageren, E. J. McInnes, and R. P. Winpenny. Direct measurement of dysprosium(III)$\cdots$ dysprosium(III) interactions in a single-molecule magnet. *Nature Communications*, 5, oct 2014.

[49] J. Du, X. Rong, N. Zhao, Y. Wang, J. Yang, and R. B. Liu. Preserving electron spin coherence in solids by optimal dynamical decoupling. *Nature*, 461(7268):1265–1268, oct 2009.

[50] M. Nechtschein, F. Genoud, C. Menardo, K. Mizoguchi, J. P. Travers, and B. Villeret. On the nature of the conducting state of polyaniline. *Synthetic Metals*, 29(1):211–218, mar 1989.

[51] T. Gaebel, M. Domhan, I. Popa, C. Wittmann, P. Neumann, F. Jelezko, J. R. Rabeau, N. Stavrias, A. D. Greentree, S. Prawer, J. Meijer, J. Twamley, P. R. Hemmer, and J. Wrachtrup. Room-temperature coherent coupling of single spins in diamond. *Nature Physics*, 2(6):408–413, 2006.

[52] D. E. Kaplan, M. E. Browne, and J. A. Cowen. Pulsed X-band EPR spectrometer. *Review of Scientific Instruments*, 32(11):1182–1186, 1961.

[53] I. Tkach, K. Halbmair, C. Höbartner, and M. Bennati. High-frequency 263 GHz PELDOR. *Applied Magnetic Resonance*, 45(10):969–979, oct 2014.

[54] S. Takahashi, L. C. Brunel, D. T. Edwards, J. Van Tol, G. Ramian, S. Han, and M. S. Sherwin. Pulsed electron paramagnetic resonance spectroscopy powered by a free-electron laser. *Nature*, 489(7416):409–413, sep 2012.

[55] J. S. Hyde, R. A. Strangeway, T. G. Camenisch, J. J. Ratke, and W. Froncisz. W-band frequency-swept EPR. *Journal of Magnetic Resonance*, 205(1):93–101, jul 2010.

[56] D. G. Mitchell, R. W. Quine, M. Tseitlin, V. Meyer, S. S. Eaton, and G. R. Eaton. Comparison of continuous wave, spin echo, and rapid scan EPR of irradiated fused quartz. *Radiation Measurements*, 46(9):993–996, sep 2011.

[57] A. Marko O. Laguta, A. Sojka and P. Neugebauer. Rapid scan esr: a versatile tool for the spin relaxation studies at (sub)thz frequencies. *accepeted in Applied Physics Letters*, 2022.

[58] J. W. Stoner, D. Szymanski, S. S. Eaton, R. W. Quine, G. A. Rinard, and G. R. Eaton. Direct-detected rapid-scan epr at 250mhz. *Journal of Magnetic Resonance*, 170(1):127–135, 2004.

[59] M. Tuček. Frequency-swept rapid-scan epr on organic radicals, 2018.

[60] M. Tseitlin, G. A. Rinard, R. W. Quine, S. S. Eaton, and G. R. Eaton. Deconvolution of sinusoidal rapid epr scans. *Journal of Magnetic Resonance*, 208(2):279–283, 2011.

[61] M. Tseitlin. General solution for rapid scan epr deconvolution problem. *Journal of Magnetic Resonance*, 318:106801, 2020.

[62] K. Möbius and A. Savitsky. *High-Field EPR Spectroscopy on Proteins and their Model Systems*. Royal Society of Chemistry, dec 2008.

[63] P. F. Goldsmith. *Quasioptical Systems: Gaussian Beam Quasioptical Propogation and Applications (IEEE Press Series on RF and Microwave Technology)*. 1998.

[64] C. Kutter, H. P. Moll, J. Van Tol, H. Zuckermann, J. C. Maan, and P. Wyder. Electron-spin echoes at 604 GHz using far infrared lasers. *Phys. Rev. Lett.*, 74(15):2925–2928, 1995.

[65] G. M. Smith, P. A. S. Cruickshank, D. R. Bolton, and D. A. Robertson. High-field pulse epr instrumentation. In *Electron Paramagnetic Resonance: Volume 21*, volume 21, pages 216–233. The Royal Society of Chemistry, 2008.

[66] Ch. Caspers, P. F. da Silva, M. Soundararajan, M. A. Haider, and J.-P. Ansermet. Field and frequency modulated sub-THz electron spin resonance spectrometer. *APL Photonics*, 1(2):026101, may 2016.

[67] A. Sojka, M. Šedivý, A. Lagiň, A. Gabriš, T. Láznička, V. T. Santana, O. Laguta, and P. Neugebauer. Sample holders for sub-thz electron spin resonance spectroscopy. *IEEE Transactions on Instrumentation and Measurement*, submitted 1/2022.

[68] L. Song, Z. Liu, P. Kaur, J. M. Esquiaqui, R. I. Hunter, S. Hill, G. M. Smith, and G. E. Fanucci. Toward increased concentration sensitivity for continuous wave epr investigations of spin-labeled biological macromolecules at high fields. *Journal of Magnetic Resonance*, 265:188–196, 2016.

[69] E. N. Yuri, A. Gopinath, and D. D. Thomas. Aqueous sample in an epr cavity: sensitivity considerations. *Journal of Magnetic Resonance*, 167(1):138–146, 2004.

[70] F. El Hallak, P. Neugebauer, A.-L. Barra, J. Van Slageren, M. Dressel, and A. Cornia. Torque-detected ESR of a tetrairon(III) single molecule magnet. *Journal of Magnetic Resonance*, 223:55–60, oct 2012.

[71] R. P. Sartoris, V. T. Santana, Eleonora F., R. F. Baggio, O. R. Nascimento, and . Calvo. Exchange couplings and quantum phases in two dissimilar arrays of similar copper dinuclear units. *Dalton Transactions*, 49(16):5228–5240, apr 2020.

[72] T. Yamane, K. Sugisaki, T. Nakagawa, H. Matsuoka, T. Nishio, S. Kinjyo, N. Mori, S. Yokoyama, C. Kawashima, N. Yokokura, K. Sato, Y. Kanzaki, D. Shiomi, K. Toyota, D. H. Dolphin, W.-C. Lin, Ch. A. McDowell, M. Tadokoro, and T. Takui. Analyses of sizable ZFS and magnetic tensors of high spin metallocomplexes. *Phys. Chem. Chem. Phys.*, 19(36):24769–24791, sep 2017.

[73] M. Simenas, A. Kultaeva, S. Balciunas, M. Trzebiatowska, D. Klose, G. Jeschke, M. Maczka, J. Banys, and A. Poppl. Single Crystal Electron Paramagnetic Resonance of Dimethylammonium and Ammonium Hybrid Formate Frameworks: Influence of External Electric Field. *Journal of Physical Chemistry C*, 121(30):16533–16540, aug 2017.

[74] V. T. Santana, B. N. Cunha, A. M. Plutín, R. G. Silveira, E. E. Castellano, A. A. Batista, R. Calvo, and O. R. Nascimento. Magnetic-field-tuned phase transition of a molecular material from the isolated-spin to the coupled-spin regime. *Phys. Chem. Chem. Phys.*, 21:4394–4407, 2019.

[75] D. Bloos, J. Kunc, L. Kaeswurm, R. L. Myers-Ward, K. Daniels, M. Dejarld, A. Nath, J. Van Slageren, D. K. Gaskill, and P. Neugebauer. Contactless millimeter wave method for quality assessment of large area graphene. *2D Materials*, 6(3):035028, may 2019.

[76] J. Ekin. Experimental Techniques for Low-Temperature Measurements: Cryostat Design, Material Properties and Superconductor Critical-Current Testing. *Experimental Techniques for Low-Temperature Measurements: Cryostat Design, Material Properties and Superconductor Critical-Current Testing*, 9780198570547:1–704, oct 2006.

[77] L. Marie, A. Fatimy, J. Hrubý, I. Nemec, J. Hunt, R. Myers-Ward, D.-K. Gaskill, M. Kruskopf, Y. Yang, R. Elmquist, R. Marx, J. Slageren, P. Neugebauer, and P. Barbara. Nanostructured graphene for nanoscale electron paramagnetic resonance spectroscopy. *Journal of Physics: Materials*, 3(1):014013, jan 2020.

[78] L. Kormoš, P. Procházka, A.-O. Makoveev, and J. Čechal. Complex k-uniform tilings by a simple bitopic precursor self-assembled on Ag(001) surface. *Nature Communications 2020 11:1*, 11(1):1–6, apr 2020.

[79] J. Hrubý, V. T. Santana, D. Kostiuk, M. Bouček, S. Lenz, M. Kern, P. Šiffalovič, J. van Slageren, and P. Neugebauer. A graphene-based hybrid material with quantum bits prepared by the double langmuir–schaefer method. *RSC Adv.*, 9:24066–24073, 2019.

[80] F. Ciccullo, M. Glaser, M.-S. Sättele, S. Lenz, P. Neugebauer, Y. Rechkemmer, J. van Slageren, and M.B. Casu. Thin film properties and stability of a potential molecular quantum bit based on copper(ii). *J. Mater. Chem. C*, 6:8028–8034, 2018.

[81] O. Laguta, A. Sojka, A. Marko, and P. Neugebauer. Rapid scan esr: a versatile tool for the spin relaxation studies at (sub)thz frequencies. *accepeted in Applied Physics Letters*, 2022.

[82] H. Sato, L. A. Dalton, D. Ha, R. W. Quine, S. S. Eaton, and G. R. Eaton. Electron spin relaxation in x-lithium phthalocyanine. *The Journal of Physical Chemistry B*, 111(28):7972–7977, 2007.

[83] G. Ilangovan, Jay L. Zweier, and P. Kuppusamy. Electrochemical preparation and epr studies of lithium phthalocyanine. *The Journal of Physical Chemistry B*, 104(40):9404–9410, 2000.

[84] S. S. Eaton and G. R. Eaton. Epr spectra and electron spin relaxation of o_2. *Applied Magnetic Resonance*, 52(10):1223–1236, 2021.